frontiers | Frontiers in Medicine

TYPE Review
PUBLISHED 25 April 2023
DOI 10.3389/fmed.2023.1060940

OPEN ACCESS

EDITED BY
Mark O. Wielpütz,
Heidelberg University, Germany

REVIEWED BY
Francesca Pennati,
Polytechnic University of Milan, Italy
Jonathan P. Dyke,
Cornell University, United States

*CORRESPONDENCE
Chuan T. Foo
✉ chuan.foo@monash.edu

RECEIVED 04 October 2022
ACCEPTED 03 April 2023
PUBLISHED 25 April 2023

CITATION
Foo CT, Langton D, Thompson BR and Thien F (2023) Functional lung imaging using novel and emerging MRI techniques. *Front. Med.* 10:1060940. doi: 10.3389/fmed.2023.1060940

Functional lung imaging using novel and emerging MRI techniques

Chuan T. Foo[1,2]*, David Langton[2,3], Bruce R. Thompson[4] and Francis Thien[1,2]

[1]Department of Respiratory Medicine, Eastern Health, Melbourne, VIC, Australia, [2]Faculty of Medicine, Nursing and Health Sciences, Monash University, Melbourne, VIC, Australia, [3]Department of Thoracic Medicine, Peninsula Health, Frankston, VIC, Australia, [4]Melbourne School of Health Science, Melbourne University, Melbourne, VIC, Australia

Respiratory diseases are leading causes of death and disability in the world. While early diagnosis is key, this has proven difficult due to the lack of sensitive and non-invasive tools. Computed tomography is regarded as the gold standard for structural lung imaging but lacks functional information and involves significant radiation exposure. Lung magnetic resonance imaging (MRI) has historically been challenging due to its short T2 and low proton density. Hyperpolarised gas MRI is an emerging technique that is able to overcome these difficulties, permitting the functional and microstructural evaluation of the lung. Other novel imaging techniques such as fluorinated gas MRI, oxygen-enhanced MRI, Fourier decomposition MRI and phase-resolved functional lung imaging can also be used to interrogate lung function though they are currently at varying stages of development. This article provides a clinically focused review of these contrast and non-contrast MR imaging techniques and their current applications in lung disease.

KEYWORDS

fluorinated gas, hyperpolarized gas, magnetic resonance imaging, oxygen-enhanced, technique, perfusion, phased-resolved functional lung imaging, ventilation heterogeneity

Introduction

Respiratory diseases impose an immense worldwide health burden (1–5). As a global measure, traditional lung function tests such as spirometry, e.g., forced expiratory volume in 1 s (FEV_1) are insensitive to early stage disease, regional heterogeneity, and subtle changes over time. Despite these limitations, spirometry and FEV_1 remain the default clinical standard for the diagnosis and assessment of various lung diseases such as asthma and chronic obstructive pulmonary disease (COPD), as well as an intermediate endpoint in longitudinal studies and clinical trials. Traditional high resolution computed tomography (HRCT) is regarded as the gold standard for structural lung imaging, but does not routinely provide much functional information. While contemporary CT-techniques such as Xenon-CT are able to assess regional lung ventilation (6), its use is currently limited to research settings. Ventilation-perfusion (VQ) scintigraphy and single-photon emission computed tomography (SPECT) (7) are other currently available methods of assessing lung ventilation but suffer from low spatial resolution and long acquisition times. Most importantly, unlike magnetic resonance imaging (MRI), all the

aforementioned techniques involve ionizing-radiation, limiting its use in patient groups such as pregnant women and children, and in situations where frequent repeated imaging is required even with low-dose CT protocols (8, 9). Despite being radiation-free, lung MRI has historically been challenging for the following reasons: (i) low proton density of lung tissue; (ii) rapid signal decay due to multiple interfaces between air and soft-tissue structures; and (iii) motion artefacts generated by cardiac, vascular and respiratory motion (10). These factors greatly reduce the signal-to-noise ratio of images acquired, resulting in the lungs appearing as dark, signal voids.

Recent advances in lung MRI have expanded its use in certain pulmonary disorders (11). Inhaled contrast agents such as hyperpolarized (HP) gases have permitted the assessment of lung ventilation, microstructure, and alveolar-capillary diffusion (12). Functional lung MRI is also possible using inhaled fluorinated gases (13), oxygen-enhanced techniques (14), and free-breathing proton methods (15, 16). Together, these novel and emerging techniques have generated a wealth of new information regarding the structure–function relationships of various lung diseases.

This review sets out to describe the most common approaches to ventilation imaging using MRI-based techniques. Each section contains a brief overview of the principles and physics behind each imaging modality, followed by a review of its current and potential clinical applications to various lung disease including but not limited to asthma, COPD, interstitial lung disease (ILD), cystic fibrosis (CF) and COVID-19. This review is divided into two main sections. First, we discuss HP-MRI, the most mature and well-established of these methods. Second, we describe the alternate and emerging techniques including fluorinated gas MRI, oxygen-enhanced MRI and free-breathing proton MRI. We conclude by examining the advantages and limitations of various techniques, and consider future directions. As this review is written with the clinician in mind, detailed technical discussions are beyond the scope of this article. Likewise, perfusion imaging will not be covered.

Hyperpolarised gas MRI

Basics of hyperpolarization

Hyperpolarization of noble gases involves the transfer of angular momentum from circularly polarized light to the noble gas nuclei, significantly increasing the atomic nuclei alignment. This results in a 10^4–10^5-fold increase in the magnetic resonance (MR) signal, enabling gases such as helium-3 (^{3}He) and xenon-129 (^{129}Xe) to be imaged despite their low levels of intrinsic polarization. Hyperpolarization can be achieved by either spin-exchange optical pumping (17) or metastability exchange optical pumping (18), with the former more commonly used in practice, and polarization levels of ~20–50% easily attainable for ^{3}He (19, 20) and ^{129}Xe (21, 22). Although this will not be discussed further, the interested reader is referred to references (23, 24) for additional information.

It is worth noting that hyperpolarization is not limited to noble gases and has also been achieved with carbon-13 (^{13}C). HP ^{13}C MRI allows *in-vivo* probing of enzyme-mediated metabolic processes such as cancers and metabolic diseases, and an excellent review of this topic can be found here (25–27).

Hardware

Polarizers crucial for the production of HP gas can be custom built (28–32) or purchased from commercial companies such as Polarean and Xemed LLC (33, 34). Dedicated transceiver coils tuned to the resonance frequency of the gas nucleus of interest are also required. MRI scanners must also be upgraded with broad-band capabilities.

Transportation

Depolarization of HP gas is accelerated by the presence of paramagnetic oxygen, magnetic field inhomogeneities, and atomic interactions between HP gas and the storage cell. The use of specialized transport equipment can overcome these challenges, facilitating long distance transportation of HP gas (35, 36).

Gas delivery

A typical inhalation mixture consists of 200–300 mL of HP gas diluted with medical-grade nitrogen in a Tedlar bag to make up a 1 L volume. Inhalation occurs from end-expiration via a mouthpiece, with images acquired under breath hold conditions of roughly 10–20 s. Addition of an exhalation circuit facilitates collection and recycling of exhaled ^{3}He.

Safety profile

Both ^{3}He and ^{129}Xe are extremely safe in the small quantities as used during HP-MRI. Other than possible transient minor oxygen desaturation observed shortly after inhalation, no serious adverse events have been described (37).

Xenon has anesthetic properties at a sustained minimum alveolar concentration of 63–71% (38, 39), but these levels are not attainable with current HP-MRI protocols. Nonetheless, ^{129}Xe has been shown to be extremely safe even after inhalation of three times the usual dose, with only mild and fleeting symptoms such as dizziness, paresthesia, euphoria and hypoesthesia being reported (40).

Noble Gas availability

^{3}He has a low natural abundance and is derived primarily from the radioactive decay of tritium (41), but much of its supply is redirected toward usage as a neutron detector (42, 43). ^{129}Xe, an isotope of xenon, has a natural abundance of 26%. An enriched ^{129}Xe mixture is often used in HP ^{129}Xe MRI to help improve the MR signal. Enriched xenon costs about A$310/L compared to A$45/L for 26% ^{129}Xe natural abundance mixture (12). The scarcity and exorbitant cost of ^{3}He, together with the fact that dissolved phase imaging is exclusively limited to ^{129}Xe has prompted the shift toward its use in recent years.

Pulmonary functional imaging approaches

Static ventilation imaging

HP-MRI permits the direct visualization of the distribution and heterogeneity of lung ventilation (Figure 1) (44). Ventilation defects represent areas of signal void (absence of HP gas) and are commonly quantified using ventilation defect percentage (VDP) or ventilated volume percentage (VV%) (45–49). VDP is calculated by dividing the ventilation defect volume (VDV) by the thoracic cavity volume, and VV% represents the inverse of VDP. Ventilation heterogeneity is best assessed using signal intensity binning (48, 50, 51), and ventilation coefficient of variation calculations (52, 53). Due to its increased sensitivity, HP ^{129}Xe MRI may identify clinically relevant ventilation defects that would otherwise be missed by ^{3}He (54, 55).

Dynamic ventilation imaging

Compared to static ventilation which provides a snap-shot of the pulmonary gas distribution pattern during a single breath-hold, dynamic ventilation allows us to study the time-dependent distribution of gas within the lungs over the entire respiratory cycle (56–58). As image acquisition begins right before inspiration, a slight modification in the gas delivery process is required, with various protocols in use (56, 57, 59). One such protocol required subjects to inhale the HP gas mixture over the first half, and exhale over the second half of a 15 s acquisition period (56).

Dynamic ventilation is able to provide information on the rate and filling patterns of the central and peripheral airways (60), individual lung lobes, and in some cases, the extent of diaphragmatic excursion. Dynamic ventilation in healthy volunteers is characterized by the uniform distribution of HP-gas throughout the lungs during inspiration, followed by a homogeneous decline in signal intensity on expiration. In contrast, heterogeneous filling pattern of lung lobes, different gas inflow rates and achieved maximum signal intensities, as well as limitation in diaphragmatic excursion due to hyperinflation are some of the findings in those with lung disease (56, 57, 59, 61–63).

Multiple-breath HP gas MRI is in essence dynamic ventilation imaging performed over multiple breath cycles. During each breath, a fraction of the HP gas is replaced by newly arrived gas, and as sequential scans are acquired at each subsequent breath-hold, a volume fractional ventilation measure is calculated by computing the rate of change in HP gas MRI signal intensity during wash-in and/or wash-out breath maneuvers (64–67). As a quantitative measure of

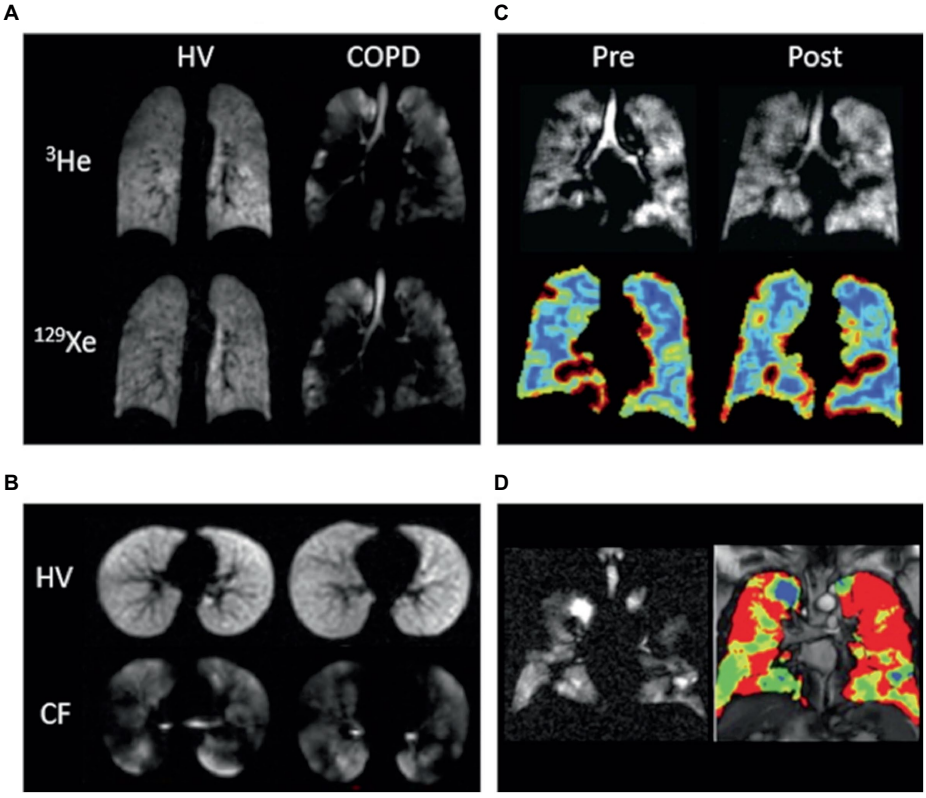

FIGURE 1
Ventilation imaging. **(A)** ^{3}He and ^{129}Xe ventilation images of a healthy non-smoker (HV) and a patient with chronic obstructive pulmonary disease (COPD). **(B)** ^{129}Xe ventilation images of a healthy 6-year-old (HV, FEV1=95%) and an 11-year-old with cystic fibrosis (CF, FEV1=102%). **(C)** ^{129}Xe ventilation images (top) and coefficient of variation maps (bottom; blue =low COV, red=high COV) of a patient with asthma pre-and post-bronchodilator inhalation. **(D)** ^{129}Xe ventilation image (left) and binning map (right; red=defect, yellow=low intensity, green=medium intensity, blue =high intensity) from an older patient with asthma (FEV1=53%). In this case, ventilation defect percentage is defined as the ratio of the number of red pixels to the total number of pixels in the whole lung×100. Adapted with permission from (23).

regional ventilation, fractional ventilation mapping is able to elucidate delayed ventilation and gas trapping in certain lung diseases.

Diffusion-weighted imaging

Diffusion-weighted imaging (DWI) exploits the high free diffusivity of ^{3}He and ^{129}Xe (68, 69) to probe the lung microstructure (70). Diffusion is quantified using the apparent diffusion coefficient (ADC), and visually represented on an ADC map with higher values suggestive of enlarged alveoli/emphysema (71, 72). Other acinar airway morphological parameters such as surface-area-to-volume-ratio, alveolar radii and mean diffusive length scale (LmD) can also be derived, and serve as additional biomarkers of lung microstructure (Figure 2) (70, 74–76). Although ADC values obtained using ^{129}Xe and ^{3}He are not directly comparable, studies have shown them to provide similar information (54, 77, 78).

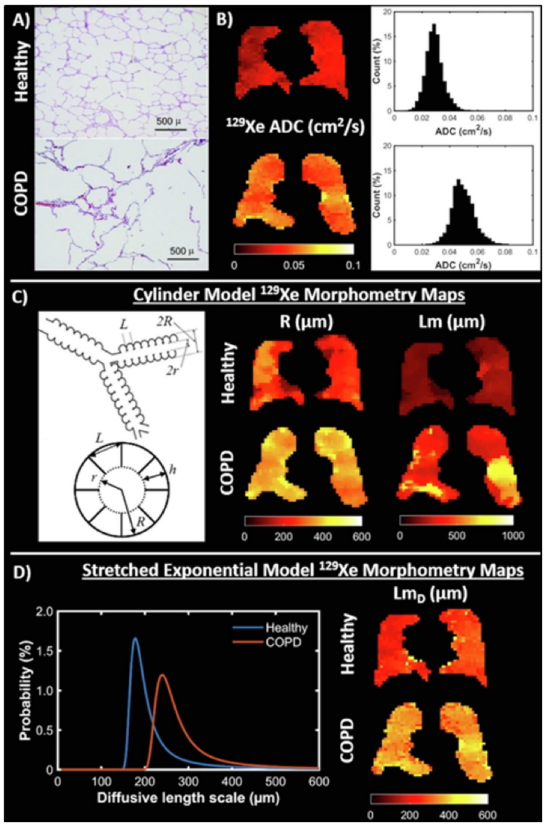

FIGURE 2
Diffusion imaging. **(A)** Examples of histological slides from a healthy lung (top) and lung with emphysema (bottom) that are used to calculate mean linear intercept (Lm) measurements. **(B)** ^{129}Xe ADC maps and whole lung ADC histograms for a healthy volunteer (23-year-old female, top) and chronic obstructive pulmonary disease (COPD) patient (68-year-old male, bottom). **(C)** (Left) Schematic drawing of the cylindrical model of acinar airway geometry based upon the Haefeli-Bleuer and Weibel acinar geometry (73). **(C)** (Right) Cylinder model ^{129}Xe lung morphometry maps of acinar airway radius (R) and mean linear intercept (Lm) in the same healthy volunteer and COPD patient as in **(B)**. **(D)** (Left) Probability distributions of diffusive length scale derived from the stretched exponential model for the same healthy volunteer and COPD patient. **(D)** (Right) Stretched exponential model ^{129}Xe lung morphometry maps of mean diffusive length scale (Lm_D) for the same healthy volunteer and COPD patient. Adapted with permission from (23).

Dissolved phase imaging

After inhalation, majority of HP ^{129}Xe remains in the gas phase, with ~2% dissolved in the lung parenchyma/plasma (barrier) and blood (RBC). At each of these transitions, ^{129}Xe exhibits a chemical shift in its resonance frequency relative to the gas phase by 197 ppm and 218 ppm in the barrier and RBC phase (79, 80). MR spectroscopy (81, 82), chemical shift saturation recovery and chemical shift imaging techniques (22, 83, 84) are able to distinguish these changes, allowing gas-exchange to be quantified as the signal ratios of ^{129}Xe within each compartment, or by alveolar morphological parameters such as septal wall thickness (Figure 3) (21, 85–89).

A summary of these biomarkers is provided in Table 1. Reference values are based on currently available data as large-scale population studies are lacking.

Clinical applications

Asthma

In the absence of treatment changes or external factors, many of the ventilation defects seen in asthmatics tend to either persist in the same location over time, or intermittently affect predictable spatial locations (19, 49, 100–103) even after an interval of 6 years (104). Furthermore, while the number and size of ventilation defects, and ventilation heterogeneity increases following bronchoprovocation (53, 101, 105–107), the locations of these defects are found to be highly reproducible regardless of the method of bronchoprovocation, suggesting a predilection for certain airways to be affected in asthma (108). Taken together, these findings suggest that ventilation abnormalities in asthma are neither widespread nor homogeneous, but regionally heterogeneous.

Ventilation defects have been associated with airway remodeling and mucus plugging. Using computed tomography (CT), bronchial wall thickening, a hallmark of airway remodeling, and gas trapping, an indirect measure of airflow obstruction, can be directly assessed, and found to correlate spatially and quantitatively with ventilation defects on HP-MRI (109, 110). Likewise, a correlation between higher mucus plugs quantified using CT (111), increased markers of gas trapping, and greater VDP have similarly been reported in asthmatics (112–114), raising the possibility that ventilation defects may be a consequence of proximal airway mucus occlusion with distal gas trapping.

Airway inflammation may also contribute to ventilation defects. Asthmatic subjects with high sputum eosinophils were observed to have a greater number of ventilation defects than those with lower counts (115). Significant correlation between increased ventilation defects and higher blood eosinophil count (116), sputum eosinophilia (115–117), fraction of exhaled nitric oxide (49, 106, 109), and neutrophils on bronchoalveolar lavage (110) have also been reported. How airway inflammation causes ventilation defects remain unclear, and has been postulated to involve increased mucus production and reduced mucus clearance (111, 118, 119). Yet, not all mucus plugs are

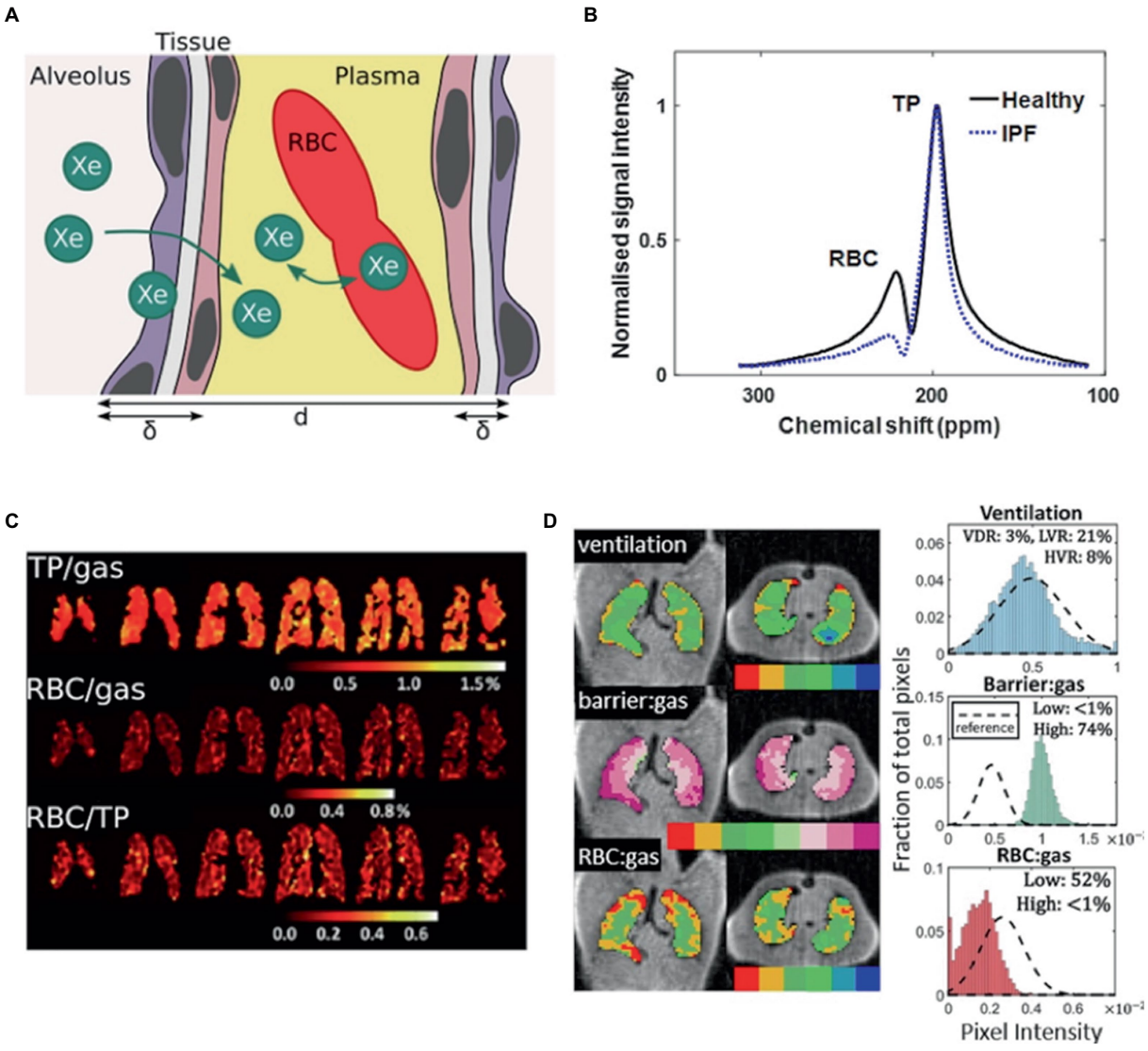

FIGURE 3
Probing gas exchange. **(A)** Cartoon of diffusive exchange of xenon gas from alveolus to capillary, via the parenchymal tissue barrier. The tissue wall thickness (air-blood barrier thickness) is represented by δ, and the total septal wall thickness separating neighboring alveoli is represented by *d*. **(B)** ^{129}Xe MR spectra obtained from a healthy subject (black line) and a patient with idiopathic pulmonary fibrosis (IPF) (blue line). **(C)** Iterative Decomposition of water/fat using Echo Asymmetry and Least-squares estimation (IDEAL) chemical shift imaging of dissolved ^{129}Xe in the lungs of a patient with moderate chronic obstructive pulmonary disease, illustrated in the form of ratio maps. **(D)** Representative binning maps and histograms derived from Dixon-based dissolved-phase ^{129}Xe MRI acquired from a patient with IPF, highlighting the characteristic high TP (barrier) signal and low RBC signal compared with healthy normal subjects (dashed histogram). (The notation barrier: gas is equivalent to TP/Gas). Adapted with permission from (23).

associated with airway inflammation (114). Similarly, the relative contributions of airway remodeling and mucus plugging toward ventilation defects are difficult to assess, and likely variable between individuals (120).

Clinically, ventilation defects have also been associated with asthma severity (45, 121), poorer asthma control and lower quality of life measures (122), even in those with milder disease (117). Similarly, higher VDP was associated with increased asthma exacerbations requiring hospitalizations (116), and higher exacerbation frequency (117). HP-MRI has also been shown to be more sensitive to asthma disease activity than subjective symptoms and spirometry, with ventilation defects observed in asthmatics with normal lung function who are asymptomatic or minimally symptomatic (19, 45). The minimum clinically important difference for VDV and VDP has recently been proposed (123), but lacks validation. Improvements in ventilation defects and overall ventilation heterogeneity have consistently been described in asthmatic subjects following treatment with bronchodilator therapy (19, 55, 115, 124), montelukast (125), after deep breathing exercises post-methacholine challenge (53), and monoclonal antibodies (126–128).

The relationship between ventilation defects and spirometric indices is complex. While numerous studies have reported significant correlations between the number of ventilation defects and FEV_1 (45, 49, 55, 105, 109, 116, 117, 121), the ratio of FEV1 to forced vital capacity (FVC) (45, 49, 55, 106, 116, 117, 121, 125), and forced expiratory flow at 25 and 50% interval (45, 49, 125), correlations with

TABLE 1 Summary of key biomarkers derived from HP-MRI.

Biomarker	Description of what it measures	Suggested reference values
VDP (VV%)	Ventilation	0–5% (95–100%) (90, 91)
CV	Regional ventilation heterogeneity	Mean CV <15% (92) IQR CV <10% (90)
ADC	Alveolar size	^{3}He: 0.1–0.3 cm^2/s (46, 71, 78, 93–96) ^{129}Xe: 0.03–0.04 cm^2/s (77, 78, 97, 98)
LmD	Alveolar size	^{3}He: 212 ± 24 um (99) ^{129}Xe: 205 ± 23um (99)
RBC:Barrier	Gas-exchange function and parenchymal tissue thickening	Dependent on imaging technique
RBC:Gas	Gas-exchange and perfusion	Dependent on imaging technique
Barrier:Gas	Tissue thickening	Dependent on imaging technique

VDP, ventilation defect percentage; VV%, ventilated volume percentage; CV, coefficient of variation; IQR, interquartile range; ADC, apparent diffusion coefficient; LmD, mean diffusive length scale; RBC, red blood cell.

FVC (45, 49, 117, 125) and the ratio of residual volume to total lung capacity (49, 106, 121) have not always been found. Ventilation defects have likewise been shown to correlate well with advanced lung function tests such as lung clearance index (122), and forced oscillation technique-measured resistance and impedance (129). Early data also suggests airway closure to be the dominant mechanism for these poorly ventilation regions (51).

It is worth mentioning that regional ventilation abnormalities in asthma have been identified using nuclear scintigraphy from as early as the 1960s (130–133), and later on using SPECT with Technegas (134). Compared to HP-MRI, these methods are limited by their inherently low spatial resolution, long scanning time, and need for ionizing radiation; factors that impede their clinical uptake and translation.

Chronic obstructive pulmonary disease

COPD patients often demonstrate ventilation defects or regions of ventilation heterogeneity on HP-MRI (46, 47, 93, 94, 135–138). These defects improve with bronchodilator therapy (139), show little intra-day variability but change after 1 week despite stable spirometry (46). Regions of high VDP have also been found to correlate with emphysematous areas on CT (140). When used in conjunction with CT, HP-MRI is able to phenotype severity of COPD (141), and differentiate healthy volunteers from those with disease (142).

Using time-resolved breath-hold ^{3}He MRI, Marshall et al. was able to visualize ventilation defects with delayed filling in a small cohort of COPD patients. Based on the pattern of delayed filling, the authors postulated that these represent regions of collateral ventilation (143). A recent study utilizing fast dynamic ^{129}Xe MRI sequence has also reported the presence of delayed ventilation in a group of COPD patients, a finding not observed in any of the healthy volunteers in the control group (144). If validated in larger cohorts, dynamic MRI may offer additional insights into the pathophysiology of COPD, assist in the detection and localization of pulmonary air leaks (145), and provide a non-invasive alternative to the assessment of collateral ventilation in patients undergoing bronchoscopic lung volume surgery.

ADC values in emphysematous regions have been found to be ~2 times higher than in healthy lungs (54, 77, 78), and correlate well with emphysema burden on CT (146). Detection of age-related emphysema has also been described (147–151). Importantly, ADC values compare favorably to current gold standard histological measurements of alveolar size (152–154).

Early detection of emphysema has been shown using ADC (155, 156), lung morphometry (157), and alveolar wall thickness (158, 159). As a biomarker of emphysema progression, ADC was observed to increase in a small group of ex-smokers with COPD over a 2-year period despite stable FEV1 (136), making it a potential treatable trait. Intra-and inter-day reproducibility of ADC measurements have also been reported (20, 46, 94).

Compared to spirometry, ventilation biomarkers showed increased sensitivity to changes in regional ventilation (139, 160), bronchodilator therapy (139), and longitudinal lung function decline (136, 161). VDP was also predictive of COPD exacerbation requiring hospitalization (162), and longitudinal changes in St George's Respiratory Questionnaire (163). Similarly, numerous studies have revealed strong correlations between ADC and FEV1 (78, 95, 157), diffusion capacity of the lung for carbon monoxide (DLCO) (54, 77, 78) and quantitative CT (54, 146, 157, 164). Furthermore, compared to CT derived mean lung density and emphysema index, ADC demonstrated higher sensitivity at separating those with COPD from healthy subjects, and better correlation with DLCO (93, 142).

Cystic fibrosis

CF is an inherited disorder due to a mutation in the cystic fibrosis transmembrane regulator gene. The lungs are often the primary site of this disease, which is currently incurable. Using HP-MRI, ventilation defects are commonly seen in CF patients and often appear in higher numbers than healthy volunteers (165, 166). These defects are often heterogeneous and patchy, with one study reporting ~5 times more ventilation defects in CF patients (mean FEV1 66% ± 27%) compared to healthy volunteers. Importantly, CF patients with normal FEV1 were also found to have 2–4 times more ventilation defects than healthy volunteers, highlighting the superior sensitivity of HP-MRI over FEV1 (165, 167, 168).

Studies examining the relationship between VDP and spirometry have yielded mixed results, with some studies reporting a high level of correlation (169–171), and others, none (168, 172). This is not surprising given the different physiologic process that VDP and FEV1 measure. In contrast, VDP has been found to correlate well with lung clearance index (90, 166), a marker of ventilation heterogeneity that is more sensitive than conventional spirometry in the detection of mild CF (173); and exhibit

the greatest sensitivity in identifying ventilation defects in patients with early CF lung disease when compared to proton lung MRI, lung clearance index (LCI), low-dose CT and spirometry (92). As a marker of disease progression, VDP was best able to identify longitudinal changes in CF patients with normal lung function when compared to spirometry, plethysmography and LCI (174, 175).

HP-MRI has also been used to monitor treatment responses in CF patients. For example, in a two part study evaluating the effect of short-and long-term ivacaftor treatment on ventilation defects in CF patients, a 13 and 9% reduction in VDP was observed after 28 days and 48 weeks respectively, along with improvements in FEV1. Notably, VDP was also observed to improve in patients whose FEV1 remained unchanged, again demonstrating the higher sensitivity of HP-MRI over traditional spirometry (171). As expected, both VDP and FEV1 promptly returned to baseline after cessation of treatment. Similar improvements in VDP have also been reported following antibiotic therapy in CF patients hospitalized with a pulmonary exacerbation (172), and after bronchodilator with albuterol (167). Although studies examining the therapeutic response of chest physiotherapy have failed to demonstrate any overall change in the number of ventilation defects, significant differences in the spatial locations of these defects were noted post intervention (168, 169). Comparable findings have also been reported in CF patients after maximal exercise (176).

Reassuringly, intra-scan and inter-scan reproducibility of HP-MRI images have been demonstrated in stable CF cohorts over intervals ranging from 1 to 64 weeks, with ventilation defects often remaining in the same spatial location (174, 177, 178). To date, there are no studies looking at dissolved phase imaging in *CF*.

Interstitial lung disease

Most studies examining ILD have focused on dissolved phase imaging. Of the few studies examining ventilation abnormalities in ILD, increased ventilation defects (179, 180) and ventilation heterogeneity (181) have been observed.

HP-MRI DWI is sensitive to the enlarged airways (bronchiectasis) and cystic spaces (honeycombing) present in fibrotic lungs (96). Elevated ADC and LmD have been reported in individuals with idiopathic pulmonary fibrosis (IPF) and found to correlate with DLCO and CT fibrosis score (182). LmD was also noted to increase over a 12-month period while other metrics remained stable, highlighting its potential role in monitoring disease progression (182). Diffusion biomarkers may additionally have a role in differentiating fibrotic from inflammatory ILD (183).

Gas-exchange assessed using whole-lung spectroscopic measurements have revealed significantly lower ^{129}Xe RBC to barrier ratio (RBC: Barrier) (82, 184), and increased alveolar septal wall thickness in subjects with ILD compared to healthy volunteers (185), suggesting the presence of diffusion limitation. As spectroscopic methods lack spatial information, dissolved phased imaging was developed (179, 186–188), and repeatedly showed elevated ^{129}Xe barrier uptake in those with IPF (179, 188). ^{129}Xe RBC transfer was also reduced, and corresponded spatially to areas of fibrosis on CT (22, 188), though correlated poorly with CT fibrosis scores (179). The increased barrier uptake and decreased RBC transfer account for the low RBC:Barrier characteristic of subjects with IPF (22, 179, 186, 188–190).

Diffusion biomarkers correlate strongly with DLCO (82, 179, 184–186, 188, 191), and appear to be more sensitive toward longitudinal disease progression in IPF than current clinical tools (191, 192). Its repeatability has also been demonstrated over time (193, 194).

Emerging evidence support the use of Xe gas-exchange imaging in identifying areas of early/active disease in IPF that are histologically abnormal, but undetected on HRCT (179, 195). If confirmed in future studies, these at-risk regions may be the target of increased monitoring or therapeutic drug trials.

COVID-19 and other lung diseases

COVID-19 is a novel infectious disease caused by the SARS-CoV-2 virus. First detected in late 2019, it was declared a global pandemic by the World Health Organization in March 2020. Beyond the acute respiratory phase, there is emerging evidence that symptoms can persist for months after the initial infection has resolved. These individuals are said to suffer from long-COVID, with fatigue and breathlessness the two most common complaints (196, 197). Interestingly, investigations such as blood test, lung function tests, or chest imaging often do not reveal any specific explanation for these symptoms (198, 199). It is here that HP-MRI, in particular ^{129}Xe MRI, has made an impact on our understanding about the causes and diagnosis of long-COVID.

In a small study of COVID-19 patients, ^{129}Xe MRI revealed alveolar capillary diffusion limitation in all subjects 3 months after COVID-pneumonia hospitalization despite normal or near normal CT and DLCO (200). These findings build on an earlier study that examined COVID-19 patients <1 month after discharge (201) and alludes to the possible etiology of persistent respiratory symptoms after the initial infection. Similar findings have also been reported in long-COVID patients who did not require hospitalization (202). In this study by Girst et al., previously hospitalized and never hospitalized patients with long-COVID were both found to have significantly lower RBC-to-barrier ratio compared to healthy volunteers, with no difference found between groups. Given that both groups had normal spirometry, DLCO (though this was lower in the never hospitalized subgroup), and normal/near normal chest CT, these findings suggest that mild COVID-19 disease can result in persistent symptoms and gas exchange abnormalities that are undetected by conventional investigations. In a separate study, similar gas-exchange abnormalities were reported in previously hospitalized long-COVID patients, with additional evidence of small vessel pruning derived from complementary quantitative lung CT analysis (203). Overall, these results are consistent with other findings that implicate alveolar membrane thickening and pulmonary vascular dysfunction (from microthrombi or alteration in pulmonary blood flow) as possible pathophysiologic explanations for long-COVID (204, 205).

Although most attention has been directed toward gas-exchange abnormalities, ventilation defects have also been observed in long-COVID patients, implicating airways disease in the pathophysiology of long-COVID. In one study involving 76 long-COVID and 9 healthy volunteers, VDP was reported to be significantly worse in those with COVID-19 compared to healthy volunteers, and also in patients who were hospitalized at the time of their COVID-19 infection compared to those who were not (206). Furthermore, VDP was also related to 6-min walk distance and exertional SpO2, but not to quality of life or dyspnea scores (206).

^{129}Xe MRI has also revealed new insights into our understanding of various other lung diseases such as non-specific interstitial

pneumonia (180), inflammatory ILD (183), pulmonary vascular disease (207, 208), and e-cigarette smoking (209).

Other novel and emerging alternatives

Fluorinated gas MRI

Fluorine-19 lung MRI (^{19}F-MRI) was first performed in humans in 2008 (13), and uses non-toxic and naturally abundant fluorinated gases as contrast agents (210, 211). Unlike HP-MRI, hyperpolarization of ^{19}F is not required prior to imaging and dedicated ^{19}F hardware, while preferred, is not essential. Extensive signal averaging to improve image quality is also possible (212).

^{19}F gases are typically inhaled as a normoxic mixture, with perfluoropropane (PFP; C_3F_8) (210) and sulfur hexafluoride (SF_6) (211) the most commonly used gases. Unlike HP-MRI, image acquisition typically occurs after steady state equilibrium of ^{19}F has been reached. This is often achieved by having the subject continuously breath from a large volume Tedlar bag, e.g., 5 L of a mixture of 79% PFP and 21% O_2 until the bag is empty. Following this, the subject inhales from a separate Tedlar bag containing 1 L of the same PFP-O_2 mixture (213), with images acquired during a 10–15 s breath-hold. Although image acquisition is also possible without the wash-in period, i.e., subject only inhales a single breath of 1 L PFP-O_2 mixture, the resultant images are often of lower quality (214).

A homogeneous ventilation pattern is classically seen in healthy subjects (210, 214), with ventilation defects and increased ventilation heterogeneity observed in those with CF (215, 216), asthma (210), COPD (210, 217) and post lung transplantation (210). Furthermore, preliminary data suggests a strong correlation between ^{19}F-MRI VDP and FEV1 in a cohort of COPD subjects (217). Intra-and inter-session reproducibility has also been demonstrated (218, 219).

^{19}F-MRI is well suited to study wash-in and wash-out kinetics as its MR signal recovers quickly and free-breathing can be performed with normoxic gas mixtures. These properties enable the quantification of regional (215, 220, 221) and collateral ventilation in subjects with lung disease (222). ^{19}F has also recently been used to assess lung ventilation and perfusion (223, 224), with VQ-mismatches identified in subjects with COPD (225, 226).

Studies comparing ^{19}F-MRI with HP-MRI are limited. A preliminary study involving 5 healthy volunteers showed that VV, VDV and VDP measurements were similar using either ^{19}F-MRI or HP-^{3}He-MRI despite ^{19}F images being of much poorer resolution (227). In contrast, a separate study of 3 healthy volunteers comparing ^{19}F-MRI with HP-^{129}Xe-MRI reported a lower VV% and CV in ^{19}F measurements when compared to ^{129}Xe, with the differences attributed to the lower observed signal with ^{19}F (228). More recently, McCallister et al. showed that while both ^{19}F-MRI and HP-^{129}Xe-MRI were able to identify ventilation abnormalities in a small cohort of mild CF patients, these abnormalities were not entirely congruent, suggesting the added utility of ^{19}F-MRI in identifying "slowly ventilated regions," and how VDP obtained from each technique may not be equivalent (229).

Oxygen-enhanced MRI

Oxygen alters the T_1-weighted signal intensity of the pulmonary blood circulation (14, 230, 231), permitting indirect imaging of the lungs. During tidal breathing, a series of T_1-weighted images are acquired using a conventional MRI scanner during both normoxic and pure oxygen conditions (232, 233), with output data represented as T_1 maps or quantified as relative enhancement ratio or oxygen transfer function (OTF) (Figure 4) (235). Using these metrics, individuals with CF and COPD were found to exhibit a heterogeneous reduction in T_1 relaxation time compared to healthy individuals (233, 236, 237). In subjects with asthma, oxygen-enhanced MRI (OE-MRI) was sensitive to airway inflammation (238), disease severity, and showed good 1-month reproducibility and intra-observer agreement (239). Differences in T_1 signal intensity changes were also noted in subjects with a variety of pulmonary diseases including ILD (240).

OE-MRI is able to detect the therapeutic effect of bronchodilators and inhaled corticosteroids in individuals with COPD (241), and been found to be comparable to quantitative CT in assessing pulmonary function loss and disease severity in individuals with COPD (242, 243), asthma (244) and connective tissue disease-ILD (245). Moreover, in subjects undergoing lung volume reduction surgery, OE-MRI was shown to be at least equivalent, if not superior to multidetector CT and SPECT in the evaluation of post-operative clinical outcomes (246). OTF has also been proposed as a potential early marker of chronic lung allograft dysfunction (247). Despite underestimating VDP, OE-MRI was reported to correlate well with ^{3}He VDP (248). VQ assessment using OE-MRI has also been described (14, 249).

Free-breathing proton MRI

The development of proton MRI functional lung imaging was driven by the need for a more accessible method of assessing lung function that did not involve complex experimental set-up, or additional costly equipment such as dedicated transmit-receiver coils and multi-nuclear capable MRI scanners.

Early researchers showed that it is possible to image the lung using MRI (without any additional special equipment or contrast agents) if a fast acquisition sequence is combined with a low magnetic field and non-rigid image registration. By applying simple signal subtraction, regional lung ventilation could be quantified, and ventilation maps generated (250).

Fourier-decomposition MRI (FD-MRI) is an innovative approach that permits the simultaneous imaging of lung ventilation and perfusion (15). FD-MRI works on the principle that changes in lung density during the respiratory and cardiac cycle create an oscillation in the MR signal that is converted into ventilation and perfusion-weighted maps by Fourier transformation (250, 251). As with all proton MRI lung imaging techniques, successful FD-MRI relies on the use of low TE sequences (below 1 msec) to reduce signal decay, and non-rigid image registration to compensate for the changes in the shape of the lungs throughout the respiratory cycle (15).

FD-MRI is able to identify ventilation defects in subjects with asthma and COPD, with FD-MRI VDP correlating strongly with ^{3}He MRI VDP (252, 253). FD-MRI VDP was also found to decrease post salbutamol and increase after inhaled methacholine in asthmatics (253), and correlated well with pulmonary function test and CT measurements in those with COPD (252). A strong correlation between FD-derived fractional ventilation and ^{19}F washout has also been described (254), and reproducibility previously established (255).

Phase-resolved functional lung MRI (PREFUL) is another unique approach that shares similarities to FD-MRI (16), with both methods

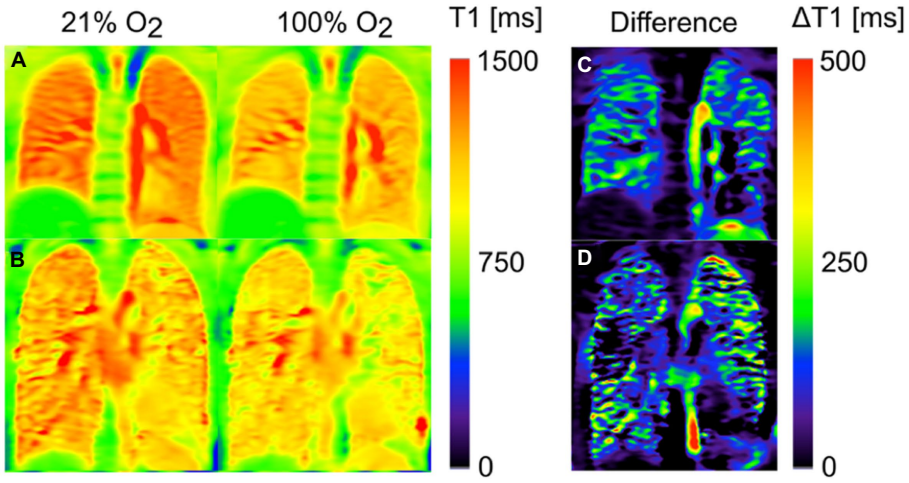

FIGURE 4
Oxygen-enhanced MRI T1 maps of a healthy volunteer **(A)** and a patient with cystic fibrosis (CF) **(B)** after inhalation of 21 and 100% oxygen. The third column shows the corresponding difference maps: While a homogenous reduction of T1(100% O2) in comparison with T1(21% O2) is found for the healthy volunteer **(C)**, some regions of the CF patient **(D)** show no or only small changes. Assuming that this effect can be mainly ascribed to reduced regional oxygen supply, the difference map can be interpreted as a surrogate for ventilation. Adapted with permission from (234).

providing an indirect quantification of ventilation and perfusion based on oscillations of the MR signal intensity within the lungs of a freely breathing subject. Whereas FD-MRI uses only the signal change amplitude to quantify these measures, PREFUL also considers the phase-component and hence the name "phase-resolved" functional lung imaging. The result is a set of phase-resolved ventilation and perfusion cycles with an increased temporal resolution compared to conventional FD-MRI.

Several ventilation and perfusion parameters can be derived from PREFUL ventilation and perfusion maps. These include regional ventilation, ventilation derived by cross-correlation, VDP, perfusion (arbitrary units), quantified perfusion, perfusion defect percentages and VQ match maps (16, 256–258).

In the feasibility trial, PREFUL was able to distinguish healthy individuals from those with lung disease (16). COPD patients were subsequently showed to have an increased number of ventilation and perfusion defects, greater ventilation heterogeneity, and higher VQ mismatch compared to healthy volunteers (258, 259). PREFUL was also able to discriminate healthy CF patients from those experiencing an exacerbation (260), and track changes in regional ventilation following treatment (259, 261). PREFUL derived regional flow volume loops also showed increased sensitivity to early stages of chronic lung allograft dysfunction (CLAD) in subjects post lung transplantation (257), and was predictive of CLAD related death or transplant loss in a large prospective cohort (262). In contrast, conventional flow volume parameters failed to show any significant difference between healthy lung transplants and early-stage CLAD (263). Likewise, PREFUL has been successfully used to study post-treatment changes in those with COPD (Figure 5) (259) and chronic thromboembolic pulmonary hypertension (CTEPH) (265), and show good agreement when compared to SPECT, dynamic contrast-enhanced-MRI, and ^{129}Xe MRI (260, 266–268).

The described techniques have so far been limited to 2D imaging although 3D modalities such as 3D PREFUL (269) and SENCEFUL (270) have recently been developed, and show promise. For instance, early 3D PREFUL data suggests a strong correlation between 3D ventilation parameters and spirometric measurements (269, 271). Additionally, repeatability of this method has also been demonstrated (258, 271). As these methods are in the early phases of development, further research is needed before they can be translated to clinical practice.

Without detracting too much from the focus of this review, PREFUL derived perfusion measures have been used to study a variety of cohorts including healthy subjects and those with COPD, CTEPH and CF (16, 256, 258, 272, 273). Validation against dynamic contrast-enhanced MRI (256, 273, 274), and repeatability have also been demonstrated (258).

Conclusion and outlook

In this review, we discuss four unique methods of functional lung imaging using MRI: (1) HP-MRI; (2) ^{19}F-MRI; (3) OE-MRI; (4) FD-MRI and PREFUL. HP-MRI is a well-established, safe and tolerable method for assessing lung function that is considered the functional lung MRI reference standard. By directly visualizing and quantifying the inhaled gas distribution, HP-MRI provides a direct assessment of lung ventilation in contrast to OE-MRI, FD-MRI and PREFUL. HP-MRI has exhibited immense potential in (i) phenotyping disease, (ii) assessing treatment response, (iii) early detection, and (iv) longitudinal monitoring. The high sensitivity (55, 275–277) and repeatability of HP-MRI biomarkers may enable future clinical trials to be undertaken with smaller sample sizes (125, 171). Emerging evidence also support its role in guiding bronchial thermoplasty (278, 279) and placement of endobronchial valves (280, 281). While diffusion-weighted and gas-exchange imaging are at an earlier stage of development, we believe they will develop into its full potential over time. Standardization of scanning protocols is essential before multi-center trials can be conducted, with guidance provided by the ^{129}Xe MRI Clinical Trials Consortium (282). While ^{129}Xe MRI has been

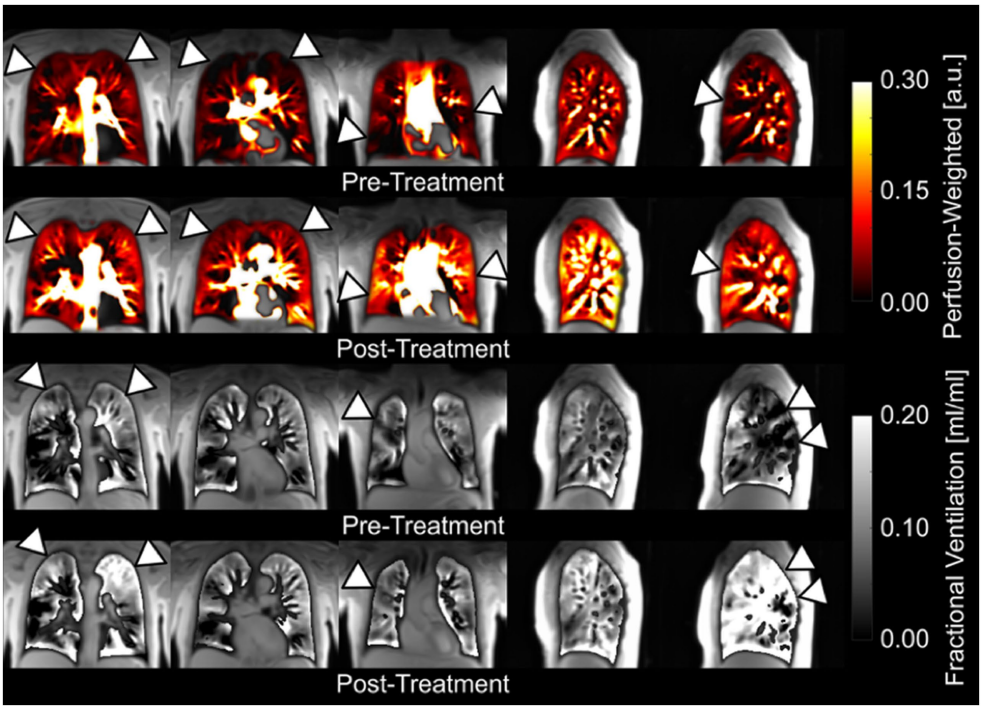

FIGURE 5
Coronal and sagittal fractional ventilation and perfusion-weighted maps of a patient with chronic obstructive pulmonary disease obtained with a free-breathing, contrast agent-free method (PREFUL) pre-and post-14 days of inhaler treatment (264). Please note the visible improvements (arrowheads) in perfusion and ventilation after treatment and the possibility for a pixelwise ventilation-perfusion assessment. Adapted with permission from (234).

approved for routine clinical use in the United Kingdom since 2015 (283), it remained limited to clinical research in the United States up until December 2022 when it received United States Food and Drug Administration approval for use in ventilation imaging (33). These represent important milestones in its broader adoption. The fact that a typical ^{129}Xe MRI examination can be easily undertaken within 5–15 min allows for seamless integration into current imaging workflows, although the high setup cost (due to expensive polarizers, dedicated coils and xenon gas), complex imaging protocol, and need for skilled personnel (to run the polarizer, administer the xenon gas and acquire images) has limited its use to dedicated research institutes and may pose barriers to future uptake. While the development of a portable ^{129}Xe hyperpolarizer shows promise as a cost-effective platform for wider clinical dissemination of ^{129}Xe MRI (284), additional unanswered questions remain about how such a service will be funded, where they will be located, which patient groups should be referred, what constitutes normal values, and in what format results will be conveyed to referring clinicians. Looking ahead, ^{129}Xe MRI may be used to distinguish a range of cardiopulmonary disorders (186, 189, 190) by analyzing cardiogenic signal oscillations arising from ^{129}Xe dissolved in the pulmonary circulation (81). The complementary use of other imaging modalities may likewise create powerful diagnostic tools to enhance our understanding of various lung diseases such as COVID-19 (201, 203, 285).

^{19}F-MRI has been touted as a possible alternative to HP-MRI given it also provides a direct measure of ventilation but at a lower operational cost – expensive polarizers are not required and fluorinated gases are less costly than HP-gases. Furthermore, due to its rapid signal recovery and ease of administration as normoxic gas mixtures, ^{19}F-MRI excels in multi-breath imaging and the study of wash-in and wash-out kinetics. Despite these advantages, the wider adoption of ^{19}F-MRI has been hindered by several factors. Firstly, ^{19}F-MRI is currently restricted to ventilation imaging (286–290), with ^{19}F lung diffusion weighted MRI still in the pre-clinical phase (288–290). Secondly, ongoing technical advances focusing on optimizing image acquisition, image quality and improving signal-to-noise ratio is required. Thirdly, rigorous reproducibility and validation studies in various patient groups are lacking, and would be needed to build up the evidence base for its use. Lastly, in this era of climate change, one must acknowledge that inert fluorinated gases, which are also utilized in many other industries, are potent greenhouse gases with long lifetimes (291). While the contribution from ^{19}F-MRI is likely to be small, efforts to capture and recycle exhaled ^{19}F gases, similar to those available for HP gases, should be pursued (292). As ^{19}F-MRI technology advances, there is strong potential for its wider clinical use.

OE-MRI also suffers from poor image and spatial resolution. More importantly, interpretation of results can be challenging due to the influence of supplemental oxygen on pulmonary physiology, and the difficulty in teasing out which of ventilation, perfusion, or diffusion is responsible for the signal changes (237, 293). Long acquisition times are also problematic, and substantial work is still required to define its role in pulmonary functional imaging.

FD-MRI and PREFUL offer a promising, cost attractive, and patient friendly alternative to functional lung imaging as imaging can be undertaken on a standard MRI scanner without the need for any additional costly equipment, or breath-holding maneuvers that are often challenging for patients with lung disease (272). The short scanning time of a couple of minutes is also beneficial for less cooperative patients such as children (294). These attributes have enabled PREFUL to be successfully employed in the assessment of

TABLE 2 Summary of the key differences between techniques.

	HP-MRI	^{19}F-MRI	OE-MRI	FD-MRI/PREFUL
Implementation				
Set-up cost	++++	+++	+	+
Skilled personnel	++++	+++	+	+
Post-processing	++++	++++	++++	++++
Aspects of lung function assessed				
Ventilation	Yes	Yes	Yes*	Yes*
Microstructure	Yes	No	No	No
Gas exchange	Yes	No	Possibly†	No
Perfusion	No	No	Possibly†	Yes
Patient factors				
Breath-hold requirement	Yes‡	Yes‡	No	No
Scanning time	+	++	+++	+
Ionizing radiation	No	No	No	No
Image resolution				
Spatial resolution	++++	+++	+	+++
Temporal resolution	NA	NA	+	++++

^{19}F, fluorine-19; FD, Fourier decomposition; HP, hyperpolarized gas; MRI, magnetic resonance imaging; OE, oxygen-enhanced; PREFUL, phased-resolved functional lung.
*These methods can only provide an indirect measure of ventilation.
†Signal derived from OE-MRI represents a combination of ventilation, diffusion and perfusion.
‡Limited or no breath hold may be possible with dynamic ventilation.

healthy, and premature infants with bronchopulmonary dysplasia, without the need for procedural sedation (295, 296). Compared to HP-MRI and ^{19}F-MRI, FD-MRI and PREFUL provide an indirect assessment of ventilation. Although ventilation biomarkers derived from these methods appear to show less sensitivity to diseased states, there is overall good agreement with HP-MRI (253, 260, 261, 268). Free-breathing MRI also has the advantage of producing detailed perfusion maps (273, 297, 298), a feature that is lacking with the other modalities. While image acquisition with free-breathing MRI is relatively easy, considerable post-processing analyses is required to generate regional functional maps. Despite this, among all the other described techniques, free-breathing MRI has possibly the lowest barrier to entry. This will be a major advantage in its scalability and transition to the clinic. A summary of the key differences between these techniques can be found in Table 2.

Compared to other functional imaging techniques such as CT, VQ and SPECT, the biggest advantage of the abovementioned MRI-techniques is that they are all free from ionizing radiation. This make these methods friendly for use in vulnerable populations such as children and pregnant women, as well as in longitudinal studies where repeated imaging is required. Moreover, there is now a growing body of evidence that these functional MRI techniques are more sensitive than current clinical endpoints such as spirometry, and may one day be used in its place.

In conclusion, novel MRI approaches to functional lung imaging offer a range of powerful and creative tools to interrogate lung function in ways that surpass current clinical methods. Despite being at different stages of maturity, these techniques all show tremendous potential in helping us better understand the structure–function relationships in a variety of lung diseases.

Author contributions

DL, BT, and FT: conceptualization. CF: data curation and writing of original draft. CF and FT: formal analysis. CF, DL, BT, and FT: review and approval of final version. All authors contributed to the article and approved the submitted version.

Funding

CF is the recipient of a Monash University post graduate scholarship.

Conflict of interest

The authors declare that the research was conducted in the absence of any commercial or financial relationships that could be construed as a potential conflict of interest.

Publisher's note

References

1. Mortality GBDCauses of Death C. Global, regional, and national life expectancy, all-cause mortality, and cause-specific mortality for 249 causes of death, 1980-2015: a systematic analysis for the global burden of disease study 2015. *Lancet*. (2016) 388:1459–544. doi: 10.1016/S0140-6736(16)31012-1

2. Burney PG, Patel J, Newson R, Minelli C, Naghavi M. Global and regional trends in COPD mortality, 1990-2010. *Eur Respir J*. (2015) 45:1239–47. doi: 10.1183/09031936.00142414

3. WHO. Global surveillance, prevention and control of chronic respiratory diseases: a comprehensive approach. (2007). Available at: https://www.who.int/gard/publications/GARD_Manual/en/

4. The Global Asthma Report. Auckland, New Zealand. (2018). Available at: http://globalasthmareport.org/

5. Ma X, Zhu L, Kurche JS, Xiao H, Dai H, Wang C. Global and regional burden of interstitial lung disease and pulmonary sarcoidosis from 1990 to 2019: results from the global burden of disease study 2019. *Thorax*. (2022) 77:596–605. doi: 10.1136/thoraxjnl-2020-216732

6. Kong X, Sheng HX, Lu GM, Meinel FG, Dyer KT, Schoepf UJ, et al. Xenon-enhanced dual-energy CT lung ventilation imaging: techniques and clinical applications. *Am J Roentgenol*. (2014) 202:309–17. doi: 10.2214/AJR.13.11191

7. Bourhis D, Robin P, Essayan M, Abgral R, Querellou S, Tromeur C, et al. V/Q SPECT for the assessment of regional lung function: generation of Normal mean and standard deviation 3-D maps. *Front Med (Lausanne)*. (2020) 7:143. doi: 10.3389/fmed.2020.00143

8. Larke FJ, Kruger RL, Cagnon CH, Flynn MJ, McNitt-Gray MM, Wu X, et al. Estimated radiation dose associated with low-dose chest CT of average-size participants in the National Lung Screening Trial. *AJR Am J Roentgenol*. (2011) 197:1165–9. doi: 10.2214/AJR.11.6533

9. Kubo T, Ohno Y, Nishino M, Lin PJ, Gautam S, Kauczor HU, et al. Low dose chest CT protocol (50 mAs) as a routine protocol for comprehensive assessment of intrathoracic abnormality. *Eur J Radiol Open*. (2016) 3:86–94. doi: 10.1016/j.ejro.2016.04.001

10. Wielputz M, Kauczor HU. MRI of the lung: state of the art. *Diagn Interv Radiol*. (2012) 18:344–53. doi: 10.4261/1305-3825.DIR.5365-11.0

11. Hatabu H, Ohno Y, Gefter WB, Parraga G, Madore B, Lee KS, et al. Expanding applications of pulmonary MRI in the clinical evaluation of lung disorders: Fleischner society position paper. *Radiology*. (2020) 297:286–301. doi: 10.1148/radiol.2020201138

12. Stewart NJ, Smith LJ, Chan HF, Eaden JA, Rajaram S, Swift AJ, et al. Lung MRI with hyperpolarised gases: current & future clinical perspectives. *Br J Radiol*. (2021) 95:20210207. doi: 10.1259/bjr.20210207

13. Wolf U, Scholz A, Terekhov M, Muennemann K., Kreitner K., Werner C., et al. Fluorine-19 MRI of the lung: first human experiment. In: *International Society for Magnetic Resonance Imaging Proceedings*; Toronto, Ontario, Canada. (2008).

14. Edelman RR, Hatabu H, Tadamura E, Li W, Prasad PV. Noninvasive assessment of regional ventilation in the human lung using oxygen-enhanced magnetic resonance imaging. *Nat Med*. (1996) 2:1236–9. doi: 10.1038/nm1196-1236

15. Bauman G, Puderbach M, Deimling M, Jellus V, Chefd'hotel C, Dinkel J, et al. Non-contrast-enhanced perfusion and ventilation assessment of the human lung by means of fourier decomposition in proton MRI. *Magn Reson Med*. (2009) 62:656–64. doi: 10.1002/mrm.22031

16. Voskrebenzev A, Gutberlet M, Klimes F, Kaireit TF, Schonfeld C, Rotarmel A, et al. Feasibility of quantitative regional ventilation and perfusion mapping with phase-resolved functional lung (PREFUL) MRI in healthy volunteers and COPD, CTEPH, and CF patients. *Magn Reson Med*. (2018) 79:2306–14. doi: 10.1002/mrm.26893

17. Bouchiat MA, Carver TR, Varnum CM. Nuclear polarization inHe^3 gas induced by optical pumping and dipolar exchange. *Phys Rev Lett*. (1960) 5:373–5. doi: 10.1103/PhysRevLett.5.373

18. Colegrove FD, Schearer LD, Walters GK. Polarization of He^3 gas by optical pumping. *Phys Rev*. (1963) 132:2561–72. doi: 10.1103/PhysRev.132.2561

19. Altes TA, Powers PL, Knight-Scott J, Rakes G, Platts-Mills TA, de Lange EE, et al. Hyperpolarized 3He MR lung ventilation imaging in asthmatics: preliminary findings. *J Magn Reson Imaging*. (2001) 13:378–84. doi: 10.1002/jmri.1054

20. Morbach AE, Gast KK, Schmiedeskamp J, Dahmen A, Herweling A, Heussel CP, et al. Diffusion-weighted MRI of the lung with hyperpolarized helium-3: a study of reproducibility. *J Magn Reson Imaging*. (2005) 21:765–74. doi: 10.1002/jmri.20300

21. Ruppert K, Mata JF, Brookeman JR, Hagspiel KD, Mugler IJP. Exploring lung function with hyperpolarized ^{129}Xe nuclear magnetic resonance. *Magn Reson Med*. (2004) 51:676–87. doi: 10.1002/mrm.10736

22. Kaushik SS, Robertson SH, Freeman MS, He M, Kelly KT, Roos JE, et al. Single-breath clinical imaging of hyperpolarized (129)Xe in the airspaces, barrier, and red blood cells using an interleaved 3D radial 1-point Dixon acquisition. *Magn Reson Med*. (2016) 75:1434–43. doi: 10.1002/mrm.25675

23. Marshall H, Stewart NJ, Chan HF, Rao MD, Norquay G, Wild JM. In vivo methods and applications of xenon-129 magnetic resonance. *Prog*. (2021) 122:42–62. doi: 10.1016/j.pnmrs.2020.11.002

24. Kauczor H, Surkau R, Roberts T. MRI using hyperpolarized noble gases. *Eur Radiol*. (1998) 8:820–7. doi: 10.1007/s003300050479

25. Wang ZJ, Ohliger MA, Larson PEZ, Gordon JW, Bok RA, Slater J, et al. Hyperpolarized (13)C MRI: state of the art and future directions. *Radiology*. (2019) 291:273–84. doi: 10.1148/radiol.2019182391

26. Vaeggemose M, F Schulte R, Laustsen C. Comprehensive literature review of hyperpolarized Carbon-13 MRI: the road to clinical application. *Metabolites*. (2021) 11:219. doi: 10.3390/metabo11040219

27. Jorgensen SH, Bogh N, Hansen E, Vaeggemose M, Wiggers H, Laustsen C. Hyperpolarized MRI – an update and future perspectives. *Semin Nucl Med*. (2022) 52:374–81. doi: 10.1053/j.semnuclmed.2021.09.001

28. Nikolaou P, Coffey AM, Walkup LL, Gust BM, LaPierre CD, Koehnemann E, et al. A 3D-printed high power nuclear spin polarizer. *J Am Chem Soc*. (2014) 136:1636–42. doi: 10.1021/ja412093d

29. Nikolaou P, Coffey AM, Walkup LL, Gust BM, Whiting N, Newton H, et al. Near-unity nuclear polarization with an open-source 129Xe hyperpolarizer for NMR and MRI. *Proc Natl Acad Sci U S A*. (2013) 110:14150–5. doi: 10.1073/pnas.1306586110

30. Nikolaou P, Coffey AM, Walkup LL, Gust BM, Whiting N, Newton H, et al. XeNA: an automated 'open-source' (129)Xe hyperpolarizer for clinical use. *Magn Reson Imaging*. (2014) 32:541–50. doi: 10.1016/j.mri.2014.02.002

31. Leawoods J, Yablonskiy D, Saam B, Gierada D, Conradi M. Hyperpolarized 3He gas production and MR imaging of the lung. *Concepts Magn Reson*. (2001) 13:277–93. doi: 10.1002/cmr.1014

32. Lee WT, Zheng G, Talbot CL, Tong X, D'Adam T, Parnell SR, et al. Hyperpolarised gas filling station for medical imaging using polarised (129)Xe and (3)He. *Magn Reson Imaging*. (2021) 79:112–20. doi: 10.1016/j.mri.2021.02.010

33. Polarean. Polarean Inc. (n.d.). Available at: https://polarean.com/

34. Xemed. Xemed LLC. (n.d.). Available at: https://www.xemed.com/

35. van Beek EJ, Schmiedeskamp J, Wild JM, Paley MN, Filbir F, Fichele S, et al. Hyperpolarized 3-helium MR imaging of the lungs: testing the concept of a central production facility. *Eur Radiol*. (2003) 13:2583–6. doi: 10.1007/s00330-003-2094-2

36. Thien F, Friese M, Cowin G, Maillet D, Wang D, Galloway G, et al. Feasibility of functional magnetic resonance lung imaging in Australia with long distance transport of hyperpolarized helium from Germany. *Respirology*. (2008) 13:599–602. doi: 10.1111/j.1440-1843.2008.01262.x

37. Lutey BA, Lefrak SS, Woods JC, Tanoli T, Quirk JD, Bashir A, et al. Hyperpolarized He-3 MR imaging: physiologic monitoring observations and safety considerations in 100 consecutive subjects. *Radiology*. (2008) 248:655–61. doi: 10.1148/radiol.2482071838

38. Cullen SC, Eger EI 2nd, Cullen BF, Gregory P. Observations on the anesthetic effect of the combination of xenon and halothane. *Anesthesiology*. (1969) 31:305–9. doi: 10.1097/00000542-196910000-00003

39. Nakata Y, Goto T, Ishiguro Y, Terui K, Kawakami H, Santo M, et al. Minimum alveolar concentration (MAC) of xenon with sevoflurane in humans. *Anesthesiology*. (2001) 94:611–4. doi: 10.1097/00000542-200104000-00014

40. Driehuys B, Martinez-Jimenez S, Cleveland ZI, Metz GM, Beaver DM, Nouls JC, et al. Chronic obstructive pulmonary disease: safety and tolerability of hyperpolarized 129Xe MR imaging in healthy volunteers and patients. *Radiology*. (2012) 262:279–89. doi: 10.1148/radiol.11102172

41. Physics CA. Helium-3 shortage could put freeze on low-temperature research. *Science*. (2009) 326:778–9. doi: 10.1126/science.326_778

42. Roos JE, McAdams HP, Kaushik SS, Driehuys B. Hyperpolarized gas MR imaging: technique and applications. *Magn Reson Imaging Clin N Am*. (2015) 23:217–29. doi: 10.1016/j.mric.2015.01.003

43. Walkup LL, Woods JC. Translational applications of hyperpolarized He-3 and Xe-129. *NMR Biomed*. (2014) 27:1429–38. doi: 10.1002/nbm.3151

44. Kauczor HU, Hofmann D, Kreitner KF, Nilgens H, Surkau R, Heil W, et al. Normal and abnormal pulmonary ventilation: visualization at hyperpolarized He-3 MR imaging. *Radiology*. (1996) 201:564–8. doi: 10.1148/radiology.201.2.8888259

45. De Lange EE, Altes TA, Patrie JT, Gaare JD, Knake JJ, Mugler IJP, et al. Evaluation of asthma with hyperpolarized helium-3 MRI: correlation with clinical severity and spirometry. *Chest*. (2006) 130:1055–62. doi: 10.1378/chest.130.4.1055

46. Mathew L, Evans A, Ouriadov A, Etemad-Rezai R, Fogel R, Santyr G, et al. Hyperpolarized He-3 magnetic resonance imaging of chronic obstructive pulmonary disease: reproducibility at 3.0 tesla. *Acad Radiol*. (2008) 15:1298–311. doi: 10.1016/j.acra.2008.04.019

47. Mathew L, Kirby M, Etemad-Rezai R, Wheatley A, McCormack DG, Parraga G. Hyperpolarized He-3 magnetic resonance imaging: preliminary evaluation of phenotyping potential in chronic obstructive pulmonary disease. *Eur J Radiol*. (2011) 79:140–6. doi: 10.1016/j.ejrad.2009.10.028

48. Kirby M, Heydarian M, Svenningsen S, Wheatley A, McCormack DG, Etemad-Rezai R, et al. Hyperpolarized He-3 magnetic resonance functional imaging Semiautomated segmentation. *Acad Radiol*. (2012) 19:141–52. doi: 10.1016/j.acra.2011.10.007

49. Ebner L, He M, Virgincar RS, Heacock T, Kaushik SS, Freemann MS, et al. Hyperpolarized 129Xenon magnetic resonance imaging to quantify regional ventilation differences in mild to moderate asthma: a prospective comparison between Semiautomated ventilation defect percentage calculation and pulmonary function tests. *Investig Radiol*. (2017) 52:120–7. doi: 10.1097/RLI.0000000000000322

50. He M, Driehuys B, Que LG, Huang YT. Using hyperpolarized (129)Xe MRI to quantify the pulmonary ventilation distribution. *Acad Radiol*. (2016) 23:1521–31. doi: 10.1016/j.acra.2016.07.014

51. Nilsen K, Thompson BR, Zajakovski N, Kean M, Harris B, Cowin G, et al. Airway closure is the predominant physiological mechanism of low ventilation seen on hyperpolarized helium-3 MRI lung scans. *J Appl Physiol*. (2021) 130:781–91. doi: 10.1152/japplphysiol.00163.2020

52. Virgincar RS, Cleveland ZI, Kaushik SS, Freeman MS, Nouls J, Cofer GP, et al. Quantitative analysis of hyperpolarized 129Xe ventilation imaging in healthy volunteers and subjects with chronic obstructive pulmonary disease. *NMR Biomed*. (2013) 26:424–35. doi: 10.1002/nbm.2880

53. Tzeng YS, Lutchen K, Albert M. The difference in ventilation heterogeneity between asthmatic and healthy subjects quantified using hyperpolarized 3He MRI. *J Appl Physiol*. (2009) 106:813–22. doi: 10.1152/japplphysiol.01133.2007

54. Kirby M, Svenningsen S, Owrangi A, Wheatley A, Farag A, Ouriadov A, et al. Hyperpolarized 3He and 129Xe MR imaging in healthy volunteers and patients with chronic obstructive pulmonary disease. *Radiology*. (2012) 265:600–10. doi: 10.1148/radiol.12120485

55. Svenningsen S, Kirby M, Starr D, Leary D, Wheatley A, Maksym GN, et al. Hyperpolarized He-3 and Xe-129 MRI: differences in asthma before bronchodilation. *J Magn Reson Imaging*. (2013) 38:1521–30. doi: 10.1002/jmri.24111

56. Salerno M, Altes TA, Brookeman JR, de Lange EE, Mugler JP 3rd. Dynamic spiral MRI of pulmonary gas flow using hyperpolarized (3)He: preliminary studies in healthy and diseased lungs. *Magn Reson Med*. (2001) 46:667–77. doi: 10.1002/mrm.1244

57. Gierada DS, Saam B, Yablonskiy D, Cooper JD, Lefrak SS, Conradi MS. Dynamic echo planar MR imaging of lung ventilation with hyperpolarized (3)He in normal subjects and patients with severe emphysema. *NMR Biomed*. (2000) 13:176–81. doi: 10.1002/1099-1492(200006)13:4<176::AID-NBM640>3.0.CO;2-I

58. Roberts DA, Rizi RR, Lipson DA, Aranda M, Baumgardner J, Bearn L, et al. Detection and localization of pulmonary air leaks using laser-polarized He-3 MRI. *Magn Reson Med*. (2000) 44:379–82. doi: 10.1002/1522-2594(200009)44:3<379::AID-MRM6>3.0.CO;2-4

59. Koumellis P, van Beek EJR, Woodhouse N, Fichele S, Swift AJ, Paley MNJ, et al. Quantitative analysis of regional airways obstruction using dynamic hyperpolarized He-3 MRI – preliminary results in children with cystic fibrosis. *J Magn Reson Imaging*. (2005) 22:420–6. doi: 10.1002/jmri.20402

60. Tooker AC, Hong KS, McKinstry EL, Costello P, Jolesz FA, Albert MS. Distal airways in humans: dynamic hyperpolarized 3He MR imaging--feasibility. *Radiology*. (2003) 227:575–9. doi: 10.1148/radiol.2272012146

61. Hahn AD, Cadman RV, Sorkness RL, Jarjour NN, Nagle SK, Fain SB. Dynamic ventilation distribution during breath-hold differs by asthma severity. In: *American journal of respiratory and critical care medicine conference: American Thoracic Society international conference*, ATS. (2013). 187 (MeetingAbstracts).

62. Doganay O, Matin TN, McIntyre A, Burns B, Schulte RF, Gleeson FV, et al. Fast dynamic ventilation MRI of hyperpolarized ^{129}Xe using spiral imaging. *Magn Reson Med*. (2018) 79:2597–606. doi: 10.1002/mrm.26912

63. Holmes JH, Korosec FR, Du J, Sorkness RL, Grist TM, Kuhlman JE, et al. Imaging of lung ventilation and respiratory dynamics in a single ventilation cycle using hyperpolarized he-3 MRI. *J Magn Reson Imaging*. (2007) 26:630–6. doi: 10.1002/jmri.20965

64. Horn FC, Deppe MH, Marshall H, Parra-Robles J, Wild JM. Quantification of regional fractional ventilation in human subjects by measurement of hyperpolarized 3He washout with 2D and 3D MRI. *J Appl Physiol*. (2014) 116:129–39. doi: 10.1152/japplphysiol.00378.2013

65. Emami K, Kadlecek SJ, Woodburn JM, Zhu JL, Yu JS, Vahdat V, et al. Improved technique for measurement of regional fractional ventilation by hyperpolarized He-3 MRI. *Magn Reson Med*. (2010) 63:137–50. doi: 10.1002/mrm.22186

66. Deninger AJ, Mansson S, Petersson JS, Pettersson G, Magnusson P, Svensson J, et al. Quantitative measurement of regional lung ventilation using 3He MRI. *Magn Reson Med*. (2002) 48:223–32. doi: 10.1002/mrm.10206

67. Hamedani H, Clapp JT, Kadlecek SJ, Emami K, Ishii M, Gefter WB, et al. Regional fractional ventilation by using multibreath wash-in (3)He MR imaging. *Radiology*. (2016) 279:917–24. doi: 10.1148/radiol.2015150495

68. Chen XJ, Moller HE, Chawla MS, Cofer GP, Driehuys B, Hedlund LW, et al. Spatially resolved measurements of hyperpolarized gas properties in the lung in vivo. Part I: diffusion coefficient. *Magn Reson Med*. (1999) 42:721–8. doi: 10.1002/(SICI)1522-2594(199910)42:4<721::AID-MRM14>3.0.CO;2-D

69. Wang J. Self-diffusion coefficients of water. *J Phys Chem*. (1965) 69:4412. doi: 10.1021/j100782a510

70. Yablonskiy DA, Sukstanskii AL, Quirk JD. Diffusion lung imaging with hyperpolarized gas MRI. *NMR Biomed*. (2017) 30:10.1002/nbm.3448. doi: 10.1002/nbm.3448

71. Saam BT, Yablonskiy DA, Kodibagkar VD, Leawoods JC, Gierada DS, Cooper JD, et al. MR imaging of diffusion of (3)He gas in healthy and diseased lungs. *Magn Reson Med*. (2000) 44:174–9. doi: 10.1002/1522-2594(200008)44:2<174::AID-MRM2>3.0.CO;2-4

72. Salerno M, Altes TA, Brookeman JR, de Lange EE, Mugler JP 3rd. Rapid hyperpolarized 3He diffusion MRI of healthy and emphysematous human lungs using an optimized interleaved-spiral pulse sequence. *J Magn Reson Imaging*. (2003) 17:581–8. doi: 10.1002/jmri.10303

73. Haefeli-Bleuer B, Weibel ER. Morphometry of the human pulmonary acinus. *Anat Rec*. (1988) 220:401–14. doi: 10.1002/ar.1092200410

74. Chan HF, Stewart NJ, Norquay G, Collier GJ, Wild JM. 3D diffusion-weighted ^{129}Xe MRI for whole lung morphometry. *Magn Reson Med*. (2018) 79:2986–95. doi: 10.1002/mrm.26960

75. Chan HF, Stewart NJ, Parra-Robles J, Collier GJ, Wild JM. Whole lung morphometry with 3D multiple b-value hyperpolarized gas MRI and compressed sensing. *Magn Reson Med*. (2017) 77:1916–25. doi: 10.1002/mrm.26279

76. Yablonskiy DA, Sukstanskii AL, Leawoods JC, Gierada DS, Bretthorst GL, Lefrak SS, et al. Quantitative in vivo assessment of lung microstructure at the alveolar level with hyperpolarized 3He diffusion MRI. *Proc Natl Acad Sci U S A*. (2002) 99:3111–6. doi: 10.1073/pnas.052594699

77. Kaushik SS, Cleveland ZI, Cofer GP, Metz G, Beaver D, Nouls J, et al. Diffusion-weighted hyperpolarized Xe-129 MRI in healthy volunteers and subjects with chronic obstructive pulmonary disease. *Magn Reson Med*. (2011) 65:1155–65. doi: 10.1002/mrm.22697

78. Stewart NJ, Chan HF, Hughes PJC, Horn FC, Norquay G, Rao M, et al. Comparison of ^{3}He and ^{129}Xe MRI for evaluation of lung microstructure and ventilation at 1.5T. *J Magn Reson Imaging*. (2018) 48:632–42. doi: 10.1002/jmri.25992

79. Mugler JP 3rd, Driehuys B, Brookeman JR, Cates GD, Berr SS, Bryant RG, et al. MR imaging and spectroscopy using hyperpolarized 129Xe gas: preliminary human results. *Magn Reson Med*. (1997) 37:809–15. doi: 10.1002/mrm.1910370602

80. Ebner L, Kammerman J, Driehuys B, Schiebler ML, Cadman RV, Fain SB. The role of hyperpolarized (129)xenon in MR imaging of pulmonary function. *Eur J Radiol*. (2017) 86:343–52. doi: 10.1016/j.ejrad.2016.09.015

81. Bier EA, Robertson SH, Schrank GM, Rackley C, Mammarappallil JG, Rajagopal S, et al. A protocol for quantifying cardiogenic oscillations in dynamic (129) Xe gas exchange spectroscopy: the effects of idiopathic pulmonary fibrosis. *NMR Biomed*. (2019) 32:e4029. doi: 10.1002/nbm.4029

82. Kaushik SS, Freeman MS, Yoon SW, Liljeroth MG, Stiles JV, Roos JE, et al. Measuring diffusion limitation with a perfusion-limited gas--hyperpolarized 129Xe gas-transfer spectroscopy in patients with idiopathic pulmonary fibrosis. *J Appl Physiol (1985)*. (2014) 117:577–85. doi: 10.1152/japplphysiol.00326.2014

83. Collier GJ, Eaden JA, Hughes PJC, Bianchi SM, Stewart NJ, Weatherley ND, et al. Dissolved ^{129}Xe lung MRI with four-echo 3D radial spectroscopic imaging: quantification of regional gas transfer in idiopathic pulmonary fibrosis. *Magn Reson Med*. (2021) 85:2622–33. doi: 10.1002/mrm.28609

84. Cleveland ZI, Cofer GP, Metz G, Beaver D, Nouls J, Kaushik SS, et al. Hyperpolarized Xe MR imaging of alveolar gas uptake in humans. *PLoS One*. (2010) 5:e12192. doi: 10.1371/journal.pone.0012192

85. Chang YV. MOXE: a model of gas exchange for hyperpolarized 129Xe magnetic resonance of the lung. *Magn Reson Med*. (2013) 69:884–90. doi: 10.1002/mrm.24304

86. Mansson S, Wolber J, Driehuys B, Wollmer P, Golman K. Characterization of diffusing capacity and perfusion of the rat lung in a lipopolysaccaride disease model using hyperpolarized 129Xe. *Magn Reson Med*. (2003) 50:1170–9. doi: 10.1002/mrm.10649

87. Ruppert K, Brookeman JR, Hagspiel KD, Mugler JP 3rd. Probing lung physiology with xenon polarization transfer contrast (XTC). *Magn Reson Med*. (2000) 44:349–57. doi: 10.1002/1522-2594(200009)44:3<349::AID-MRM2>3.0.CO;2-J

88. Patz S, Muradyan I, Hrovat M, Dabaghyan M, Washko G, Hatabu H. Diffusion of hyperpolarized 129Xe in the lung: a simplified model of 129Xe septal uptake and experimental results. *New J Phys*. (2011) 13. doi: 10.1088/1367-2630/13/1/015009

89. Ruppert K, Qing K, Altes TA, Mata JF, Ruset IC, Hersman F, et al. Septal wall thickness changes in COPD assessed by CSSR MR spectroscopy. In: *American journal of respiratory and critical care medicine conference: American Thoracic Society international conference*, ATS. (2014). 189(MeetingAbstracts).

90. Smith LJ, Collier GJ, Marshall H, Hughes PJC, Biancardi AM, Wildman M, et al. Patterns of regional lung physiology in cystic fibrosis using ventilation magnetic resonance imaging and multiple-breath washout. *Eur Respir J*. (2018) 52:1800821. doi: 10.1183/13993003.00821-2018

91. He M, Kaushik SS, Robertson SH, Freeman MS, Virgincar RS, McAdams HP, et al. Extending semiautomatic ventilation defect analysis for hyperpolarized (129)Xe ventilation MRI. *Acad Radiol*. (2014) 21:1530–41. doi: 10.1016/j.acra.2014.07.017

92. Marshall H, Horsley A, Taylor CJ, Smith L, Hughes D, Horn FC, et al. Detection of early subclinical lung disease in children with cystic fibrosis by lung ventilation imaging with hyperpolarised gas MRI. *Thorax*. (2017) 72:760–2. doi: 10.1136/thoraxjnl-2016-208948

93. Diaz S, Casselbrant I, Piitulainen E, Magnusson P, Peterson B, Wollmer P, et al. Validity of apparent diffusion coefficient hyperpolarized He-3-MRI using MSCT and pulmonary function tests as references. *Eur J Radiol*. (2009) 71:257–63. doi: 10.1016/j.ejrad.2008.04.013

94. Parraga G, Ouriadov A, Evans A, McKay S, Lam WW, Fenster A, et al. Hyperpolarized He-3 ventilation defects and apparent diffusion coefficients in chronic obstructive pulmonary disease – preliminary results at 3.0 tesla. *Investig Radiol*. (2007) 42:384–91. doi: 10.1097/01.rli.0000262571.81771.66

95. Salerno M, De Lange EE, Altes TA, Truwit JD, Brookeman JR, Mugler IJP. Emphysema: hyperpolarized helium 3 diffusion MR imaging of the lungs compared with spirometric indexes – initial experience. *Radiology*. (2002) 222:252–60. doi: 10.1148/radiol.2221001834

96. Bink A, Hanisch G, Karg A, Vogel A, Katsaros K, Mayer E, et al. Clinical aspects of the apparent diffusion coefficient in 3He MRI: results in healthy volunteers and patients after lung transplantation. *J Magn Reson Imaging*. (2007) 25:1152–8. doi: 10.1002/jmri.20933

97. Mugler J, Mata J, Wang H, Tobias W, Cates G, Christopher J, et al., The apparent diffusion coefficient of 129-Xe in the lung: preliminary human results. In: *Proceedings of the International Society for Magnetic Resonance in medicine*; Japan. (2004).

98. Sindile A, Muradian I, Hrovat M, Johnson D, Hersman F, Patz S. Human pulmonary diffusion weighted imaging at 0.2T with hyperpolarized 129Xe. In: *Proceedings of the International Society for Magnetic Resonance in medicine*; Germany. (2007).

99. Chan HF, Collier GJ, Weatherley ND, Wild JM. Comparison of in vivo lung morphometry models from 3D multiple b-value ^{3}He and ^{129}Xe diffusion-weighted MRI. *Magn Reson Med*. (2019) 81:2959–71. doi: 10.1002/mrm.27608

100. De Lange EE, Altes TA, Patrie JT, Battiston JJ, Juersivich AP, Mugler IJP, et al. Changes in regional airflow obstruction over time in the lungs of patients with asthma: evaluation with ^{3}He MR imaging. *Radiology*. (2009) 250:567–75. doi: 10.1148/radiol.2502080188

101. de Lange EE, Altes TA, Patrie JT, Parmar J, Brookeman JR, Mugler IJP, et al. The variability of regional airflow obstruction within the lungs of patients with asthma: assessment with hyperpolarized helium-3 magnetic resonance imaging. *J Allergy Clin Immunol*. (2007) 119:1072–8. doi: 10.1016/j.jaci.2006.12.659

102. Wheatley A, McKay S, Mathew L, Santyr G, McCormack DG, Parraga G. Hyperpolarized helium-3 magnetic resonance imaging of asthma: short-term reproducibility – art. No. 69161X. In: Hu XP, Clough AV, editors. *Medical imaging 2008: physiology, function, and structure from medical images. Proceedings of the Society of Photo-Optical Instrumentation Engineers (Spie)*. 6916 (2008). X9161-X.

103. Svenningsen S, Guo F, Kirby M, Choy S, Wheatley A, McCormack DG, et al. Pulmonary functional magnetic resonance imaging: asthma temporal-spatial maps. *Acad Radiol*. (2014) 21:1402–10. doi: 10.1016/j.acra.2014.08.002

104. Eddy RL, Svenningsen S, Licskai C, McCormack DG, Parraga G. Hyperpolarized helium 3 MRI in mild-to-moderate asthma: prediction of Postbronchodilator reversibility. *Radiology*. (2019) 293:212–20. doi: 10.1148/radiol.2019190420

105. Samee S, Altes T, Powers P, De Lange EE, Knight-Scott J, Rakes G, et al. Imaging the lungs in asthmatic patients by using hyperpolarized helium-3 magnetic resonance: assessment of response to methacholine and exercise challenge. *J Allergy Clin Immunol*. (2003) 111:1205–11. doi: 10.1067/mai.2003.1544

106. Costella S, Kirby M, Maksym GN, McCormack DG, Paterson NAM, Parraga G. Regional pulmonary response to a methacholine challenge using hyperpolarized He-3 magnetic resonance imaging. *Respirology*. (2012) 17:1237–46. doi: 10.1111/j.1440-1843.2012.02250.x

107. Niles DJ, Kruger SJ, Dardzinski BJ, Harman A, Jarjour NN, Ruddy M, et al. Exercise-induced bronchoconstriction: reproducibility of hyperpolarized 3He MR imaging. *Radiology*. (2013) 266:618–25. doi: 10.1148/radiol.12111973

108. Fennema M, Capaldi D, Sheikh K, Svenningsen S, Eddy R, Licskai C, et al., *The abnormal airways that dominate asthma attack: new clues using ventilation MRI during exercise and methacholine-challenge. American Thoracic Society international conference*. San Francisco. (2016).

109. Svenningsen S, Kirby M, Starr D, Coxson HO, Paterson NAM, McCormack DG, et al. What are ventilation defects in asthma? *Thorax*. (2014) 69:63–71. doi: 10.1136/thoraxjnl-2013-203711

110. Fain SB, Gonzalez-Fernandez G, Peterson ET, Evans MD, Sorkness RL, Jarjour NN, et al. Evaluation of structure-function relationships in asthma using multidetector CT and hyperpolarized He-3 MRI. *Acad Radiol*. (2008) 15:753–62. doi: 10.1016/j.acra.2007.10.019

111. Dunican EM, Elicker BM, Gierada DS, Nagle SK, Schiebler ML, Newell JD, et al. Mucus plugs in patients with asthma linked to eosinophilia and airflow obstruction. *J Clin Invest*. (2018) 128:997–1009. doi: 10.1172/JCI95693

112. Mummy D, Dunican E, Lampkins T, Zha W, Evans M, Schiebler M, et al. Ventilation defects in asthma on hyperpolarized gas MRI are associated with airway mucus plugs on CT. In: *American journal of respiratory and critical care medicine conference: American Thoracic Society international conference*, ATS. (2018);197(MeetingAbstracts).

113. Dunican E, Fahy J, Mummy DG, Fain S, Hoffman EA, Elicker BM, et al. *Regional ventilation defects measured on hyperpolarized 3He MRI are associated with mucus plugging measured on CT in asthma. American Thoracic Society international conference*; San Francisco. (2016).

114. Svenningsen S, Haider E, Boylan C, Mukherjee M, Eddy RL, Capaldi DPI, et al. CT and functional MRI to evaluate airway mucus in severe asthma. *Chest*. (2019) 155:1178–89. doi: 10.1016/j.chest.2019.02.403

115. Svenningsen S, Eddy RL, Lim HF, Cox PG, Nair P, Parraga G. Sputum eosinophilia and magnetic resonance imaging ventilation heterogeneity in severe asthma. *Am J Respir Crit Care Med*. (2018) 197:876–84. doi: 10.1164/rccm.201709-1948OC

116. Mummy DG, Kruger SJ, Zha W, Sorkness RL, Jarjour NN, Schiebler ML, et al. Ventilation defect percent in helium-3 magnetic resonance imaging as a biomarker of severe outcomes in asthma. *J Allergy Clin Immunol*. (2018) 141:1140–.e4. doi: 10.1016/j.jaci.2017.10.016

117. Mummy DG, Carey KJ, Evans MD, Denlinger LC, Schiebler ML, Sorkness RL, et al. Ventilation defects on hyperpolarized helium-3 MRI in asthma are predictive of 2-year exacerbation frequency. *J Allergy Clin Immunol*. (2020) 146:831–9.e6. doi: 10.1016/j.jaci.2020.02.029

118. Tanizaki Y, Kitani H, Okazaki M, Mifune T, Mitsunobu F, Kimura I. Mucus hypersecretion and eosinophils in bronchoalveolar lavage fluid in adult patients with bronchial asthma. *J Asthma*. (1993) 30:257–62.

119. Corcoran TE, Huber AS, Hill SL, Locke LW, Weber L, Muthukrishnan A, et al. Mucociliary clearance differs in mild asthma by levels of type 2 inflammation. *Chest*. (2021) 160:1604–13. doi: 10.1016/j.chest.2021.05.013

120. Eddy RL, Svenningsen S, Kirby M, Knipping D, McCormack DG, Licskai C, et al. Is computed tomography airway count related to asthma severity and airway structure and function? *Am J Respir Crit Care Med*. (2020) 201:923–33. doi: 10.1164/rccm.201908-1552OC

121. Zha W, Kruger SJ, Cadman RV, Mummy DG, Evans MD, Nagle SK, et al. Regional heterogeneity of lobar ventilation in asthma using hyperpolarized Helium-3 MRI. *Acad Radiol*. (2018) 25:169–78. doi: 10.1016/j.acra.2017.09.014

122. Svenningsen S, Nair P, Guo FM, McCormack DG, Parraga G. Is ventilation heterogeneity related to asthma control? *Eur Respir J*. (2016) 48:370–9. doi: 10.1183/13993003.00393-2016

123. Eddy RL, Svenningsen S, McCormack DG, Parraga G. What is the minimal clinically important difference for helium-3 magnetic resonance imaging ventilation defects? *Eur Respir J*. (2018) 51:06. doi: 10.1183/13993003.00324-2018

124. Teague WG, Tustison NJ, Altes TA. Ventilation heterogeneity in asthma. *J Asthma*. (2014) 51:677–84. doi: 10.3109/02770903.2014.914535

125. Kruger SJ, Niles DJ, Dardzinski B, Harman A, Jarjour NN, Ruddy M, et al. Hyperpolarized Helium-3 MRI of exercise-induced bronchoconstriction during challenge and therapy. *J Magn Reson Imaging*. (2014) 39:1230–7. doi: 10.1002/jmri.24272

126. Svenningsen S, Haider EA, Eddy RL, Parraga G, Nair P. Normalisation of MRI ventilation heterogeneity in severe asthma by dupilumab. *Thorax*. (2019) 74:1087–8. doi: 10.1136/thoraxjnl-2019-213415

127. Svenningsen S, Eddy RL, Kjarsgaard M, Parraga G, Nair P. Effects of anti-T2 biologic treatment on lung ventilation evaluated by MRI in adults with prednisone-dependent asthma. *Chest*. (2020) 158:1350–60. doi: 10.1016/j.chest.2020.04.056

128. Thomen R. Hyperpolarised xenon MRI in treatment of severe asthma by mepolizumab: toward earlier detection of individual patient responses (2020). Available at: https://grantome.com/grant/NIH/R01-HL152288-01

129. Young HM, Guo FM, Eddy RL, Maksym G, Parraga G. Oscillometry and pulmonary MRI measurements of ventilation heterogeneity in obstructive lung disease: relationship to quality of life and disease control. *J Appl Physiol*. (2018) 125:73–85. doi: 10.1152/japplphysiol.01031.2017

130. Siegler D, Fukuchi Y, Engel L. Influence of bronchomotor tone on ventilation distribution and airway closure in asymptomatic asthma. *Am Rev Respir Dis*. (1976) 114:123–30. doi: 10.1164/arrd.1976.114.1.123

131. Sergysels R, Scano G, Vrebos J, Bracamonte M, Vandevivere J. Effect of fenoterol on small airways and regional lung function in asymptomatic asthma. *Eur J Clin Pharmacol*. (1983) 24:429–34. doi: 10.1007/BF00609881

132. Heckscher T, Bass H, Oriol A, Rose B, Anthoniesen NR, Bates DV. Regional lung function in patients with bronchial asthma. *J Clin Invest*. (1968) 47:1063–70. doi: 10.1172/JCI105796

133. Bentivoglio LG, Beerel F, Bryan AC, Stewart PB, Rose B, Bates DV. Regional pulmonary function studied with xenon in patients with bronchial asthma. *J Clin Invest*. (1963) 42:1193–200. doi: 10.1172/JCI104805

134. King GG, Eberl S, Salome CM, Young IH, Woolcock AJ. Differences in airway closure between normal and asthmatic subjects measured with single-photon emission computed tomography and technegas. *Am J Respir Crit Care Med*. (1998) 158:1900–6. doi: 10.1164/ajrccm.158.6.9608027

135. Choy S, Wheatley A, McCormack DG, Parraga G. Hyperpolarized He-3 magnetic resonance imaging-derived pulmonary pressure-volume curves. *J Appl Physiol*. (2010) 109:574–85. doi: 10.1152/japplphysiol.01085.2009

136. Kirby M, Mathew L, Wheatley A, Santyr GE, McCormack DG, Parraga G. Chronic obstructive pulmonary disease: longitudinal hyperpolarized (3)He MR imaging. *Radiology*. (2010) 256:280–9. doi: 10.1148/radiol.10091937

137. Owrangi AM, Wang JX, Wheatley A, McCormack DG, Parraga G. Quantitative H-1 and hyperpolarized He-3 magnetic resonance imaging: comparison in chronic obstructive pulmonary disease and healthy never-smokers. *Eur J Radiol*. (2014) 83:64–72. doi: 10.1016/j.ejrad.2012.02.018

138. Yu J, Law M, Kadlecek S, Emami K, Ishii M, Stephen M, et al. Simultaneous measurement of pulmonary partial pressure of oxygen and apparent diffusion coefficient by hyperpolarized 3He MRI. *Magn Reson Med*. (2009) 61:1015–21. doi: 10.1002/mrm.21854

139. Kirby M, Mathew L, Heydarian M, Etemad-Rezai R, McCormack DG, Parraga G. Chronic obstructive pulmonary disease: quantification of bronchodilator effects by using hyperpolarized ^{3}He MR imaging. *Radiology*. (2011) 261:283–92. doi: 10.1148/radiol.11110403

140. Kirby M, Svenningsen S, Kanhere N, Owrangi A, Wheatley A, Coxson HO, et al. Pulmonary ventilation visualized using hyperpolarized helium-3 and xenon-129 magnetic resonance imaging: differences in COPD and relationship to emphysema. *J Appl Physiol*. (2013) 114:707–15. doi: 10.1152/japplphysiol.01206.2012

141. Pike D, Kirby M, Eddy RL, Guo F, Capaldi DPI, Ouriadov A, et al. Regional heterogeneity of chronic obstructive pulmonary disease phenotypes: pulmonary ^{3}He magnetic resonance imaging and computed tomography. *COPD*. (2016) 13:601–9. doi: 10.3109/15412555.2015.1123682

142. van Beek EJ, Dahmen AM, Stavngaard T, Gast KK, Heussel CP, Krummenauer F, et al. Hyperpolarised 3He MRI versus HRCT in COPD and normal volunteers: PHIL trial. *Eur Respir J*. (2009) 34:1311–21. doi: 10.1183/09031936.00138508

143. Marshall H, Deppe MH, Parra-Robles J, Hillis S, Billings CG, Rajaram S, et al. Direct visualisation of collateral ventilation in COPD with hyperpolarised gas MRI. *Thorax*. (2012) 67:613–7. doi: 10.1136/thoraxjnl-2011-200864

144. Chen MH, Doganay O, Matin T, McIntyre A, Rahman N, Bulte D, et al. Delayed ventilation assessment using fast dynamic hyperpolarised Xenon-129 magnetic resonance imaging. *Eur Radiol*. (2020) 30:1145–55. doi: 10.1007/s00330-019-06415-1

145. Roberts DA, Rizi RR, Lipson DA, Aranda M, Baumgardner J, Bearn L, et al. Detection and localization of pulmonary air leaks using laser-polarized (3)He MRI. *Magn Reson Med*. (2000) 44:379–82. doi: 10.1002/1522-2594(200009)44:3<379::AID-MRM6>3.0.CO;2-4

146. Matin TN, Rahman N, Nickol AH, Chen M, Xu XJ, Stewart NJ, et al. Chronic obstructive pulmonary disease: lobar analysis with hyperpolarized Xe-129 MR imaging. *Radiology*. (2017) 282:857–68. doi: 10.1148/radiol.2016152299

147. Altes TA, Mata J, de Lange EE, Brookeman JR, Mugler JP 3rd. Assessment of lung development using hyperpolarized helium-3 diffusion MR imaging. *J Magn Reson Imaging*. (2006) 24:1277–83. doi: 10.1002/jmri.20723

148. Fain SB, Altes TA, Panth SR, Evans MD, Waters B, Mugler JP 3rd, et al. Detection of age-dependent changes in healthy adult lungs with diffusion-weighted 3He MRI. *Acad Radiol*. (2005) 12:1385–93. doi: 10.1016/j.acra.2005.08.005

149. Gillooly M, Lamb D. Airspace size in lungs of lifelong non-smokers: effect of age and sex. *Thorax*. (1993) 48:39–43.

150. Quirk JD, Sukstanskii AL, Woods JC, Lutey BA, Conradi MS, Gierada DS, et al. Experimental evidence of age-related adaptive changes in human acinar airways. *J Appl Physiol*. (2016) 120:159–65. doi: 10.1152/japplphysiol.00541.2015

151. Waters B, Owers-Bradley J, Silverman M. Acinar structure in symptom-free adults by Helium-3 magnetic resonance. *Am J Respir Crit Care Med*. (2006) 173:847–51. doi: 10.1164/rccm.200411-1595OC

152. Thomen RP, Quirk JD, Roach D, Egan-Rojas T, Ruppert K, Yusen RD, et al. Direct comparison of Xe-129 diffusion measurements with quantitative histology in human lungs. *Magn Reson Med*. (2017) 77:265–72. doi: 10.1002/mrm.26120

153. Woods JC, Choong CK, Yablonskiy DA, Bentley J, Wong J, Pierce JA, et al. Hyperpolarized He-3 diffusion MRI and histology in pulmonary emphysema. *Magn Reson Med*. (2006) 56:1293–300. doi: 10.1002/mrm.21076

154. Yablonskiy DA, Sukstanskii AL, Woods JC, Gierada DS, Quirk JD, Hogg JC, et al. Quantification of lung microstructure with hyperpolarized 3He diffusion MRI. *J Appl Physiol*. (2009) 107:1258–65. doi: 10.1152/japplphysiol.00386.2009

155. Fain SB, Panth SR, Evans MD, Wentland AL, Holmes JH, Korosec FR, et al. Early emphysematous changes in asymptomatic smokers: detection with 3He MR imaging. *Radiology*. (2006) 239:875–83. doi: 10.1148/radiol.2393050111

156. Swift AJ, Wild JM, Fichele S, Woodhouse N, Fleming S, Waterhouse J, et al. Emphysematous changes and normal variation in smokers and COPD patients using diffusion 3He MRI. *Eur J Radiol*. (2005) 54:352–8. doi: 10.1016/j.ejrad.2004.08.002

157. Quirk JD, Lutey BA, Gierada DS, Woods JC, Senior RM, Lefrak SS, et al. *In vivo* detection of acinar microstructural changes in early emphysema with He-3 lung morphometry. *Radiology*. (2011) 260:866–74. doi: 10.1148/radiol.11102226

158. Kern AL, Gutberlet M, Qing K, Voskrebenzev A, Klimes F, Kaireit TF, et al. Regional investigation of lung function and microstructure parameters by localized (129) Xe chemical shift saturation recovery and dissolved-phase imaging: a reproducibility study. *Magn Reson Med*. (2019) 81:13–24. doi: 10.1002/mrm.27407

159. Ruppert K, Qing K, Patrie JT, Altes TA, Mugler JP 3rd. Using hyperpolarized Xenon-129 MRI to quantify early-stage lung disease in smokers. *Acad Radiol*. (2019) 26:355–66. doi: 10.1016/j.acra.2018.11.005

160. Horn FC, Marshall H, Collier GJ, Kay R, Siddiqui S, Brightling CE, et al. Regional ventilation changes in the lung: treatment response mapping by using hyperpolarized gas MR imaging as a quantitative biomarker. *Radiology*. (2017) 284:854–61. doi: 10.1148/radiol.2017160532

161. Baron RJ, Hamedani H, Kadlecek SJ, Duncan IF, Xin Y, Siddiqui S, et al. A model for predicting future FEV1 decline in smokers using hyperpolarized (3)He magnetic resonance imaging. *Acad Radiol*. (2019) 26:383–94. doi: 10.1016/j.acra.2018.06.024

162. Kirby M, Pike D, Coxson HO, McCormack DG, Parraga G. Hyperpolarized He-3 ventilation defects used to predict pulmonary exacerbations in mild to moderate chronic obstructive pulmonary disease. *Radiology*. (2014) 273:887–96. doi: 10.1148/radiol.14140161

163. Kirby M, Eddy RL, Pike D, Svenningsen S, Coxson HO, Sin DD, et al. MRI ventilation abnormalities predict quality-of-life and lung function changes in mild-to-moderate COPD: longitudinal TINCan study. *Thorax*. (2017) 72:475–7. doi: 10.1136/thoraxjnl-2016-209770

164. Tafti S, Garrison WJ, Mugler JP, Shim YM, Altes TA, Mata JF, et al. Emphysema index based on hyperpolarized He-3 or Xe-129 diffusion MRI: performance and comparison with quantitative CT and pulmonary function tests. *Radiology*. (2020) 297:201–10. doi: 10.1148/radiol.2020192804

165. Thomen RP, Walkup LL, Roach DJ, Cleveland ZI, Clancy JP, Woods JC. Hyperpolarized (129)Xe for investigation of mild cystic fibrosis lung disease in pediatric patients. *J Cyst Fibros*. (2017) 16:275–82. doi: 10.1016/j.jcf.2016.07.008

166. Kanhere N, Couch MJ, Kowalik K, Zanette B, Rayment JH, Manson D, et al. Correlation of lung clearance index with hyperpolarized (129)Xe magnetic resonance imaging in pediatric subjects with cystic fibrosis. *Am J Respir Crit Care Med*. (2017) 196:1073–5. doi: 10.1164/rccm.201611-2228LE

167. Mentore K, Froh DK, de Lange EE, Brookeman JR, Paget-Brown AO, Altes TA. Hyperpolarized HHe 3 MRI of the lung in cystic fibrosis: assessment at baseline and after bronchodilator and airway clearance treatment. *Acad Radiol*. (2005) 12:1423–9. doi: 10.1016/j.acra.2005.07.008

168. Bannier E, Cieslar K, Mosbah K, Aubert F, Duboeuf F, Salhi Z, et al. Hyperpolarized 3He MR for sensitive imaging of ventilation function and treatment efficiency in young cystic fibrosis patients with normal lung function. *Radiology*. (2010) 255:225–32. doi: 10.1148/radiol.09090039

169. Woodhouse N, Wild JM, van Beek EJ, Hoggard N, Barker N, Taylor CJ. Assessment of hyperpolarized 3He lung MRI for regional evaluation of interventional therapy: a pilot study in pediatric cystic fibrosis. *J Magn Reson Imaging*. (2009) 30:981–8. doi: 10.1002/jmri.21949

170. McMahon CJ, Dodd JD, Hill C, Woodhouse N, Wild JM, Fichele S, et al. Hyperpolarized 3helium magnetic resonance ventilation imaging of the lung in cystic fibrosis: comparison with high resolution CT and spirometry. *Eur Radiol*. (2006) 16:2483–90. doi: 10.1007/s00330-006-0311-5

171. Altes TA, Johnson M, Fidler M, Botfield M, Tustison NJ, Leiva-Salinas C, et al. Use of hyperpolarized helium-3 MRI to assess response to ivacaftor treatment in patients with cystic fibrosis. *J Cyst Fibros*. (2017) 16:267–74. doi: 10.1016/j.jcf.2016.12.004

172. Rayment JH, Couch MJ, McDonald N, Kanhere N, Manson D, Santyr G, et al. Hyperpolarised (129)Xe magnetic resonance imaging to monitor treatment response in children with cystic fibrosis. *Eur Respir J*. (2019) 53:1802188. doi: 10.1183/13993003.02188-2018

173. Aurora P, Gustafsson P, Bush A, Lindblad A, Oliver C, Wallis CE, et al. Multiple breath inert gas washout as a measure of ventilation distribution in children with cystic fibrosis. *Thorax*. (2004) 59:1068–73. doi: 10.1136/thx.2004.022590

174. Smith LJ, Horsley A, Bray J, Hughes PJC, Biancardi A, Norquay G, et al. The assessment of short-and long-term changes in lung function in cystic fibrosis using Xe-129 MRI. *Eur Respir J*. (2020) 56:2000441. doi: 10.1183/13993003.00441-2020

175. Smith L, Marshall H, Aldag I, Horn F, Collier G, Hughes D, et al. Longitudinal assessment of children with mild cystic fibrosis using hyperpolarized gas lung magnetic resonance imaging and lung clearance index. *Am J Respir Crit Care Med*. (2018) 197:397–400. doi: 10.1164/rccm.201705-0894LE

176. Smith LJ, Marshall H, Bray J, Wildman M, West N, Horsley A, et al. The effect of acute maximal exercise on the regional distribution of ventilation using ventilation MRI in CF. *J Cyst Fibros*. (2020) 20:625–31. doi: 10.1016/j.jcf.2020.08.009

177. O'Sullivan B, Couch M, Roche JP, Walvick R, Zheng S, Baker D, et al. Assessment of repeatability of hyperpolarized gas MR ventilation functional imaging in cystic fibrosis. *Acad Radiol*. (2014) 21:1524–9. doi: 10.1016/j.acra.2014.07.008

178. Kirby M, Svenningsen S, Ahmed H, Wheatley A, Etemad-Rezai R, Paterson NA, et al. Quantitative evaluation of hyperpolarized helium-3 magnetic resonance imaging of lung function variability in cystic fibrosis. *Acad Radiol*. (2011) 18:1006–13. doi: 10.1016/j.acra.2011.03.005

179. Wang JM, Robertson SH, Wang Z, He M, Virgincar RS, Schrank GM, et al. Using hyperpolarized (129)Xe MRI to quantify regional gas transfer in idiopathic pulmonary fibrosis. *Thorax*. (2018) 73:21–8. doi: 10.1136/thoraxjnl-2017-210070

180. Mummy DG, Bier EA, Wang Z, Korzekwinski J, Morrison L, Barkauskas C, et al. Hyperpolarized (129)Xe MRI and spectroscopy of gas-exchange abnormalities in nonspecific interstitial pneumonia. *Radiology*. (2021) 301:211–20. doi: 10.1148/radiol.2021204149

181. Mammarappallil JG, Rankine L, Wild JM, Driehuys B. New developments in imaging idiopathic pulmonary fibrosis with hyperpolarized xenon magnetic resonance imaging. *J Thorac Imaging*. (2019) 34:136–50. doi: 10.1097/RTI.0000000000000392

182. Chan HF, Weatherley ND, Johns CS, Stewart NJ, Collier GJ, Bianchi SM, et al. Airway microstructure in idiopathic pulmonary fibrosis: assessment at hyperpolarized 3He diffusionweighted MRI. *Radiology*. (2019) 291:223–9. doi: 10.1148/radiol.2019181714

183. Eaden JA, Collier GJ, Norquay G, Chan HF, Hughes PJC, Weatherley ND, et al. Hyperpolarised 129-xenon mri in differentiating between fibrotic and inflammatory interstitial lung disease and assessing longitudinal change. *Thorax*. (2021) 76:A46–7. doi: 10.1136/thorax-2020-BTSabstracts.80

184. Robertson SH, Virgincar RS, Bier EA, He M, Schrank GM, Smigla RM, et al. Uncovering a third dissolved-phase (129) Xe resonance in the human lung: quantifying spectroscopic features in healthy subjects and patients with idiopathic pulmonary fibrosis. *Magn Reson Med*. (2017) 78:1306–15. doi: 10.1002/mrm.26533

185. Stewart NJ, Leung G, Norquay G, Marshall H, Parra-Robles J, Murphy PS, et al. Experimental validation of the hyperpolarized Xe-129 chemical shift saturation recovery technique in healthy volunteers and subjects with interstitial lung disease. *Magn Reson Med*. (2015) 74:196–207. doi: 10.1002/mrm.25400

186. Collier GJ, Eaden JA, Hughes PJC, Bianchi SM, Stewart NJ, Weatherley ND, et al. Dissolved (129) Xe lung MRI with four-echo 3D radial spectroscopic imaging: quantification of regional gas transfer in idiopathic pulmonary fibrosis. *Magn Reson Med*. (2021) 85:2622–33. doi: 10.1002/mrm.28609

187. Qing K, Ruppert K, Jiang Y, Mata JF, Miller W, Shim YM, et al. Regional mapping of gas uptake by blood and tissue in the human lung using hyperpolarized Xenon-129 MRI. *J Magn Reson Imaging*. (2014) 39:346–59. doi: 10.1002/jmri.24181

188. Wang Z, Robertson SH, Wang J, He M, Virgincar RS, Schrank GM, et al. Quantitative analysis of hyperpolarized ^{129}Xe gas transfer MRI. *Med Phys*. (2017) 44:2415–28. doi: 10.1002/mp.12264

189. Niedbalski PJ, Bier EA, Wang Z, Willmering MM, Driehuys B, Cleveland ZI. Mapping cardiopulmonary dynamics within the microvasculature of the lungs using dissolved (129)Xe MRI. *J Appl Physiol (1985)*. (2020) 129:218–29. doi: 10.1152/japplphysiol.00186.2020

190. Wang Z, Bier EA, Swaminathan A, Parikh K, Nouls J, He M, et al. Diverse cardiopulmonary diseases are associated with distinct xenon magnetic resonance imaging signatures. *Eur Respir J*. (2019) 54:1900831. doi: 10.1183/13993003.00831-2019

191. Weatherley ND, Stewart NJ, Chan HF, Austin M, Smith LJ, Collier G, et al. Hyperpolarised xenon magnetic resonance spectroscopy for the longitudinal assessment of changes in gas diffusion in IPF. *Thorax*. (2019) 74:500–2. doi: 10.1136/thoraxjnl-2018-211851

192. Rankine LJ, Wang Z, Wang JM, He M, McAdams HP, Mammarappallil J, et al. (129)xenon gas exchange magnetic resonance imaging as a potential prognostic marker for progression of idiopathic pulmonary fibrosis. *Ann Am Thorac Soc*. (2020) 17:121–5. doi: 10.1513/AnnalsATS.201905-413RL

193. Hahn A, Carey KJ, Barton GP, Torres LA, Cadman RV, Sandbo NK, et al. *Functional MRI of regional gas exchange in IPF disease progression. American journal of respiratory and critical care medicine conference: American Thoracic Society international conference*, ATS. (2020).201.

194. Stewart NJ, Horn FC, Norquay G, Collier GJ, Yates DP, Lawson R, et al. Reproducibility of quantitative indices of lung function and microstructure from ^{129}Xe chemical shift saturation recovery (CSSR) MR spectroscopy. *Magn Reson Med*. (2017) 77:2107–13. doi: 10.1002/mrm.26310

195. Coxson HO, Hogg JC, Mayo JR, Behzad H, Whittall KP, Schwartz DA, et al. Quantification of idiopathic pulmonary fibrosis using computed tomography and histology. *Am J Respir Crit Care Med*. (1997) 155:1649–56. doi: 10.1164/ajrccm.155.5.9154871

196. Halpin SJ, McIvor C, Whyatt G, Adams A, Harvey O, McLean L, et al. Postdischarge symptoms and rehabilitation needs in survivors of COVID-19 infection: a cross-sectional evaluation. *J Med Virol*. (2021) 93:1013–22. doi: 10.1002/jmv.26368

197. Garrigues E, Janvier P, Kherabi Y, Le Bot A, Hamon A, Gouze H, et al. Post-discharge persistent symptoms and health-related quality of life after hospitalization for COVID-19. *J Infect*. (2020) 81:e4–6. doi: 10.1016/j.jinf.2020.08.029

198. Huang C, Huang L, Wang Y, Li X, Ren L, Gu X, et al. 6-month consequences of COVID-19 in patients discharged from hospital: a cohort study. *Lancet*. (2021) 397:220–32. doi: 10.1016/S0140-6736(20)32656-8

199. Torres-Castro R, Vasconcello-Castillo L, Alsina-Restoy X, Solis-Navarro L, Burgos F, Puppo H, et al. Respiratory function in patients post-infection by COVID-19: a systematic review and meta-analysis. *Pulmonology*. (2021) 27:328–37. doi: 10.1016/j.pulmoe.2020.10.013

200. Grist JT, Chen M, Collier GJ, Raman B, Abueid G, McIntyre A, et al. Hyperpolarized (129)Xe MRI abnormalities in dyspneic patients 3 months after COVID-19 pneumonia: preliminary results. *Radiology*. (2021) 301:E353–60. doi: 10.1148/radiol.2021210033

201. Li H, Zhao X, Wang Y, Lou X, Chen S, Deng H, et al. Damaged lung gas exchange function of discharged COVID-19 patients detected by hyperpolarized (129)Xe MRI. *Sci Adv*. (2021) 7:eabc8180. doi: 10.1126/sciadv.abc8180

202. Grist JT, Collier GJ, Walters H, Kim M, Chen M, Abu Eid G, et al. Lung abnormalities detected with hyperpolarized (129)Xe MRI in patients with long COVID. *Radiology*. (2022) 305:709–17. doi: 10.1148/radiol.220069

203. Matheson AM, McIntosh MJ, Kooner HK, Lee J, Desaigoudar V, Bier E, et al. Persistent (129)Xe MRI pulmonary and CT vascular abnormalities in symptomatic individuals with post-acute COVID-19 syndrome. *Radiology*. (2022) 305:466–76. doi: 10.1148/radiol.220492

204. Parra-Medina R, Herrera S, Mejia J. Systematic review of microthrombi in COVID-19 autopsies. *Acta Haematol*. (2021) 144:476–83. doi: 10.1159/000515104

205. Dimbath E, Maddipati V, Stahl J, Sewell K, Domire Z, George S, et al. Implications of microscale lung damage for COVID-19 pulmonary ventilation dynamics: a narrative review. *Life Sci*. (2021) 274:119341. doi: 10.1016/j.lfs.2021.119341

206. Kooner HK, McIntosh MJ, Matheson AM, Venegas C, Radadia N, Ho T, et al. (129)Xe MRI ventilation defects in ever-hospitalised and never-hospitalised people with post-acute COVID-19 syndrome. *BMJ Open Respir Res*. (2022) 9:e001235. doi: 10.1136/bmjresp-2022-001235

207. Dahhan T, Kaushik SS, He M, Mammarappallil JG, Tapson VF, McAdams HP, et al. Abnormalities in hyperpolarized (129)Xe magnetic resonance imaging and spectroscopy in two patients with pulmonary vascular disease. *Pulm Circ*. (2016) 6:126–31. doi: 10.1086/685110

208. Bier EA, Alenezi F, Lu J, Wang Z, Mammarappallil JG, O'Sullivan-Murphy B, et al. Noninvasive diagnosis of pulmonary hypertension with hyperpolarised (129)Xe magnetic resonance imaging and spectroscopy. *ERJ Open Res*. (2022) 8:00035-2022. doi: 10.1183/23120541.00035-2022

209. He M, Qing K, Tustison NJ, Beaulac Z, King TW, Huff TB, et al. Characterizing gas exchange physiology in healthy Young electronic-cigarette users with hyperpolarized (129)Xe MRI: a pilot study. *Int J Chron Obstruct Pulmon Dis*. (2021) 16:3183–7. doi: 10.2147/COPD.S324388

210. Halaweish AF, Moon RE, Foster WM, Soher BJ, McAdams HP, MacFall JR, et al. Perfluoropropane gas as a magnetic resonance lung imaging contrast agent in humans. *Chest*. (2013) 144:1300–10. doi: 10.1378/chest.12-2597

211. Schreiber WG, Eberle B, Laukemper-Ostendorf S, Markstaller K, Weiler N, Scholz A, et al. Dynamic (19)F-MRI of pulmonary ventilation using sulfur hexafluoride (SF(6)) gas. *Magn Reson Med*. (2001) 45:605–13. doi: 10.1002/mrm.1082

212. Kuethe DO, Pietrass T, Behr VC. Inert fluorinated gas T1 calculator. *J Magn Reson*. (2005) 177:212–20. doi: 10.1016/j.jmr.2005.07.022

213. Couch MJ, Ball IK, Li T, Fox MS, Ouriadov AV, Biman B, et al. Inert fluorinated gas MRI: a new pulmonary imaging modality. *NMR Biomed*. (2014) 27:1525–34. doi: 10.1002/nbm.3165

214. Couch MJ, Ball IK, Li T, Fox MS, Littlefield SL, Biman B, et al. Pulmonary ultrashort echo time 19F MR imaging with inhaled fluorinated gas mixtures in healthy volunteers: feasibility. *Radiology*. (2013) 269:903–9. doi: 10.1148/radiol.13130609

215. Goralski JL, Chung SH, Glass TM, Ceppe AS, Akinnagbe-Zusterzeel EO, Trimble AT, et al. Dynamic perfluorinated gas MRI reveals abnormal ventilation despite normal FEV1 in cystic fibrosis. *JCI Insight*. (2020) 5:e133400. doi: 10.1172/jci.insight.133400

216. Lee Y, Akinnagbe-Zusterzeel E, Goralski J, Donaldson S., An H., Charles H.C., et al. 19F ventilation imaging of cystic fibrosis patients. In: *Proceedings of the International Society for Magnetic Resonance in medicine*; Singapore. (2016).

217. Gutberlet M, Kaireit TF, Voskrebenzev A, Lasch F, Freise J, Welte T, et al. Free-breathing dynamic (19)F gas MR imaging for mapping of regional lung ventilation in patients with COPD. *Radiology*. (2018) 286:1040–51. doi: 10.1148/radiol.2017170591

218. Pippard BJ, Neal MA, Maunder AM, Hollingsworth KG, Biancardi A, Lawson RA, et al. Reproducibility of (19) F-MR ventilation imaging in healthy volunteers. *Magn Reson Med*. (2021) 85:3343–52. doi: 10.1002/mrm.28660

219. Gutberlet M, Kaireit TF, Voskrebenzev A, Kern AL, Obert A, Wacker F, et al. Repeatability of regional lung ventilation quantification using fluorinated ((19)F) gas magnetic resonance imaging. *Acad Radiol*. (2019) 26:395–403. doi: 10.1016/j.acra.2018.10.021

220. Gutberlet M, Kaireit T, Voskrebenzav A. Real-time dynamic fluorinated gas RI in free breathing for mapping of regional lung ventilation in patients with COPD and healthy volunteers using a 16 channel receive coil at 1.5T. In: *Proceedings of the International Society for Magnetic Resonance in medicine*. SIngapore. (2016).

221. Halaweish A, Foster W, Moon R. Dynamics of pulmonary ventilation distribution at steady state via 19 fluorine-enhanced MRI: initial experiences and future developments. In *Proceedings of the International Society for Magnetic Resonance in medicine*. USA. (2013).

222. Mammarappallil J, MacIntyre N, Mahmood K, Womack S, Cecil CH. Imaging ventilation using 19F perfluorinated gas magnetic resonance imaging: strategies for imaging collateral ventilation. *J Lung Pulm Respir Res*. (2021) 8:41–5. doi: 10.15406/jlprr.2021.08.00249

223. Adolphi NL, Kuethe DO. Quantitative mapping of ventilation-perfusion ratios in lungs by 19F MR imaging of T1 of inert fluorinated gases. *Magn Reson Med*. (2008) 59:739–46. doi: 10.1002/mrm.21579

224. Neal MA, Pippard BJ, Simpson AJ, Thelwall PE. Dynamic susceptibility contrast (19) F-MRI of inhaled perfluoropropane: a novel approach to combined pulmonary ventilation and perfusion imaging. *Magn Reson Med*. (2020) 83:452–61. doi: 10.1002/mrm.27933

225. Gutberlet M, Obert A, Voskrebenzav A, Klimes F, Wacker F, Vogel-Claussen J. Quantification of gas concentration and fractional ventilation using high temporal resolution MRI of pulmonary fluorinated (19F) gas washin dynamics in free breathing. In: *Proceedings of the International Society for Magnetic Resonance in medicine*. Paris. (2018).

226. Obert A, Gutberlet M, Rotarmel A, Wacker F, Vogel-Claussen J. Mapping of ventilation/perfusion ratios in the human lung using 19F MRI of perfluoropropane. In: *Proceedings of the International Society for Magnetic Resonance in medicine*. Paris. (2018).

227. Couch M, Ball I, Li T, Fox M, Biman B, Albert M, Comparing pulmonary MRI using inert fluorinated gases and hyperpolarized 3He: is 19F MRI good enough? In: *Proceedings of the International Society for Magnetic Resonance in medicine*; Toronto, Canada. (2015)

228. Maunder A, Hughes P, Chan H, Norquay G., Collier G., Rodgers O., et al Comparing 19F C3F8 lung ventilation imaging with hyperpolarized 129Xe: similarities and limitations. In: *Proceedings of the International Society for Magnetic Resonance in medicine*. Paris. (2018).

229. McCallister A, Chung SH, Antonacci M, Z Powell M, Ceppe AS, Donaldson SH, et al. Comparison of single breath hyperpolarized (129) Xe MRI with dynamic (19) F MRI in cystic fibrosis lung disease. *Magn Reson Med*. (2021) 85:1028–38. doi: 10.1002/mrm.28457

230. Ohno Y, Hatabu H. Basics concepts and clinical applications of oxygen-enhanced MR imaging. *Eur J Radiol*. (2007) 64:320–8. doi: 10.1016/j.ejrad.2007.08.006

231. Renne J, Lauermann P, Hinrichs J, Schonfeld C, Sorrentino S, Gutberlet M, et al. Clinical use of oxygen-enhanced T1 mapping MRI of the lung: reproducibility and impact of closed versus loose fit oxygen delivery system. *J Magn Reson Imaging*. (2015) 41:60–6. doi: 10.1002/jmri.24535

232. Hatabu H, Tadamura E, Chen Q, Stock KW, Li W, Prasad PV, et al. Pulmonary ventilation: dynamic MRI with inhalation of molecular oxygen. *Eur J Radiol*. (2001) 37:172–8. doi: 10.1016/S0720-048X(00)00298-9

233. Ohno Y, Hatabu H, Takenaka D, Van Cauteren M, Fujii M, Sugimura K. Dynamic oxygen-enhanced MRI reflects diffusing capacity of the lung. *Magn Reson Med*. (2002) 47:1139–44. doi: 10.1002/mrm.10168

234. Voskrebenzev A, Vogel-Claussen J. Proton MRI of the lung: how to tame scarce protons and fast signal decay. *J Magn Reson Imaging*. (2021) 53:1344–57. doi: 10.1002/jmri.27122

235. Brooke JP, Hall IP. Novel thoracic MRI approaches for the assessment of pulmonary physiology and inflammation. *Adv Exp Med Biol*. (2021) 1304:123–45. doi: 10.1007/978-3-030-68748-9_8

236. Kaireit TF, Sorrentino SA, Renne J, Schoenfeld C, Voskrebenzev A, Gutberlet M, et al. Functional lung MRI for regional monitoring of patients with cystic fibrosis. *PLoS One*. (2017) 12:e0187483. doi: 10.1371/journal.pone.0187483

237. Loffler R, Muller CJ, Peller M, Penzkofer H, Deimling M, Schwaiblmair M, et al. Optimization and evaluation of the signal intensity change in multisection oxygen-enhanced MR lung imaging. *Magn Reson Med*. (2000) 43:860–6. doi: 10.1002/1522-2594(200006)43:6<860::AID-MRM12>3.0.CO;2-C

238. Renne J, Hinrichs J, Schonfeld C, Gutberlet M, Winkler C, Faulenbach C, et al. Noninvasive quantification of airway inflammation following segmental allergen challenge with functional MR imaging: a proof of concept study. *Radiology*. (2015) 274:267–75. doi: 10.1148/radiol.14132607

239. Zhang WJ, Niven RM, Young SS, Liu YZ, Parker GJ, Naish JH. Dynamic oxygen-enhanced magnetic resonance imaging of the lung in asthma – initial experience. *Eur J Radiol*. (2015) 84:318–26. doi: 10.1016/j.ejrad.2014.10.021

240. Muller CJ, Schwaiblmair M, Scheidler J, Deimling M, Weber J, Loffler RB, et al. Pulmonary diffusing capacity: assessment with oxygen-enhanced lung MR imaging preliminary findings. *Radiology*. (2002) 222:499–506. doi: 10.1148/radiol.2222000869

241. Morgan AR, Parker GJ, Roberts C, Buonaccorsi GA, Maguire NC, Hubbard Cristinacce PL, et al. Feasibility assessment of using oxygen-enhanced magnetic resonance imaging for evaluating the effect of pharmacological treatment in COPD. *Eur J Radiol*. (2014) 83:2093–101. doi: 10.1016/j.ejrad.2014.08.004

242. Ohno Y, Hatabu H, Takenaka D, Adachi S, Van Cauteren M, Sugimura K. Oxygen-enhanced MR ventilation imaging of the lung: preliminary clinical experience in 25 subjects. *AJR Am J Roentgenol*. (2001) 177:185–94. doi: 10.2214/ajr.177.1.1770185

243. Ohno Y, Iwasawa T, Seo JB, Koyama H, Takahashi H, Oh YM, et al. Oxygen-enhanced magnetic resonance imaging versus computed tomography: multicenter study for clinical stage classification of smoking-related chronic obstructive pulmonary disease. *Am J Respir Crit Care Med*. (2008) 177:1095–102. doi: 10.1164/rccm.200709-1322OC

244. Ohno Y, Koyama H, Matsumoto K, Onishi Y, Nogami M, Takenaka D, et al. Oxygen-enhanced MRI vs. quantitatively assessed thin-section CT: pulmonary functional loss assessment and clinical stage classification of asthmatics. *Eur J Radiol*. (2011) 77:85–91. doi: 10.1016/j.ejrad.2009.06.027

245. Ohno Y, Nishio M, Koyama H, Yoshikawa T, Matsumoto S, Seki S, et al. Oxygen-enhanced MRI for patients with connective tissue diseases: comparison with thin-section CT of capability for pulmonary functional and disease severity assessment. *Eur J Radiol*. (2014) 83:391–7. doi: 10.1016/j.ejrad.2013.11.001

246. Ohno Y, Nishio M, Koyama H, Yoshikawa T, Matsumoto S, Takenaka D, et al. Oxygen-enhanced MRI, thin-section MDCT, and perfusion SPECT/CT: comparison of clinical implications to patient care for lung volume reduction surgery. *AJR Am J Roentgenol*. (2012) 199:794–802. doi: 10.2214/AJR.11.8250

247. Renne J, Lauermann P, Hinrichs JB, Schonfeld C, Sorrentino S, Gutberlet M, et al. Chronic lung allograft dysfunction: oxygen-enhanced T1-mapping MR imaging of the lung. *Radiology*. (2015) 276:266–73. doi: 10.1148/radiol.15141486

248. Zha W, Nagle SK, Cadman RV, Schiebler ML, Fain SB. Three-dimensional isotropic functional imaging of cystic fibrosis using oxygen-enhanced MRI: comparison with hyperpolarized (3)He MRI. *Radiology*. (2019) 290:229–37. doi: 10.1148/radiol.2018181148

249. Jobst BJ, Triphan SM, Sedlaczek O, Anjorin A, Kauczor HU, Biederer J, et al. Functional lung MRI in chronic obstructive pulmonary disease: comparison of T1 mapping, oxygen-enhanced T1 mapping and dynamic contrast enhanced perfusion. *PLoS One*. (2015) 10:e0121520. doi: 10.1371/journal.pone.0121520

250. Zapke M, Topf HG, Zenker M, Kuth R, Deimling M, Kreisler P, et al. Magnetic resonance lung function–a breakthrough for lung imaging and functional assessment? A phantom study and clinical trial. *Respir Res*. (2006) 7:106. doi: 10.1186/1465-9921-7-106

251. Deimling M, Jellus V, Geiger B, Chefd'hotel C. Time resolved lung ventilation imaging by Fourier decomposition. In: *Proceedings of the international Soceity for magnetic resonance in medicine*; Canada. (2008).

252. Capaldi DP, Sheikh K, Guo F, Svenningsen S, Etemad-Rezai R, Coxson HO, et al. Free-breathing pulmonary 1H and hyperpolarized 3He MRI: comparison in COPD and bronchiectasis. *Acad Radiol*. (2015) 22:320–9. doi: 10.1016/j.acra.2014.10.003

253. Capaldi DPI, Sheikh K, Eddy RL, Guo F, Svenningsen S, Nair P, et al. Free-breathing functional pulmonary MRI: response to bronchodilator and Bronchoprovocation in severe asthma. *Acad Radiol*. (2017) 24:1268–76. doi: 10.1016/j.acra.2017.04.012

254. Kaireit TF, Gutberlet M, Voskrebenzev A, Freise J, Welte T, Hohlfeld JM, et al. Comparison of quantitative regional ventilation-weighted fourier decomposition MRI with dynamic fluorinated gas washout MRI and lung function testing in COPD patients. *J Magn Reson Imaging*. (2018) 47:1534–41. doi: 10.1002/jmri.25902

255. Lederlin M, Bauman G, Eichinger M, Dinkel J, Brault M, Biederer J, et al. Functional MRI using Fourier decomposition of lung signal: reproducibility of ventilation-and perfusion-weighted imaging in healthy volunteers. *Eur J Radiol*. (2013) 82:1015–22. doi: 10.1016/j.ejrad.2012.12.003

256. Glandorf J, Klimes F, Behrendt L, Voskrebenzev A, Kaireit TF, Gutberlet M, et al. Perfusion quantification using voxel-wise proton density and median signal decay in PREFUL MRI. *Magn Reson Med*. (2021) 86:1482–93. doi: 10.1002/mrm.28787

257. Moher Alsady T, Voskrebenzev A, Greer M, Becker L, Kaireit TF, Welte T, et al. MRI-derived regional flow-volume loop parameters detect early-stage chronic lung allograft dysfunction. *J Magn Reson Imaging*. (2019) 50:1873–82. doi: 10.1002/jmri.26799

258. Pohler GH, Klimes F, Behrendt L, Voskrebenzev A, Gonzalez CC, Wacker F, et al. Repeatability of phase-resolved functional lung (PREFUL)-MRI ventilation and perfusion parameters in healthy subjects and COPD patients. *J Magn Reson Imaging*. (2021) 53:915–27. doi: 10.1002/jmri.27385

259. Vogel-Claussen J, Schonfeld CO, Kaireit TF, Voskrebenzev A, Czerner CP, Renne J, et al. Effect of Indacaterol/Glycopyrronium on pulmonary perfusion and ventilation in Hyperinflated patients with chronic obstructive pulmonary disease (CLAIM). A double-blind, randomized, crossover trial. *Am J Respir Crit Care Med*. (2019) 199:1086–96. doi: 10.1164/rccm.201805-0995OC

260. Couch MJ, Munidasa S, Rayment JH, Voskrebenzev A, Seethamraju RT, Vogel-Claussen J, et al. Comparison of functional free-breathing pulmonary (1)H and hyperpolarized (129)Xe magnetic resonance imaging in pediatric cystic fibrosis. *Acad Radiol*. (2021) 28:e209–18. doi: 10.1016/j.acra.2020.05.008

261. Munidasa S, Couch MJ, Rayment JH, Voskrebenzev A, Seethamraju R, Vogel-Claussen J, et al. Free-breathing MRI for monitoring ventilation changes following antibiotic treatment of pulmonary exacerbations in paediatric cystic fibrosis. *Eur Respir J*. (2021) 57:2003104. doi: 10.1183/13993003.03104-2020

262. Vogel-Claussen J, Kaireit T, Voskrebenzev A, Klimes F, Behrendt L, Gutberlet M, et al. Value of functional lung MRI in long term patient care after lung transplantation. *Eur Respir J*. (2022) 60:3778. doi: 10.1183/13993003.congress-2022.3778

263. Voskrebenzev A, Greer M, Gutberlet M, Schonfeld C, Renne J, Hinrichs J, et al. Detection of chronic lung allograft dysfunction using ventilation-weighted Fourier decomposition MRI. *Am J Transplant*. (2018) 18:2050–60. doi: 10.1111/ajt.14759

264. Vogel-Claussen J, Kaireit T, Voskrebenzev A, Schoenfeld C-O, Czerner C, Renne J, et al. Indacaterol/Glycopyrronium improves pulmonary ventilation and ventilation inhomogeneity in the CLAIM study. *Eur Respiratory Soc*. (2018) doi: 10.1183/13993003.congress-2018.PA4388

265. Pohler GH, Klimes F, Voskrebenzev A, Behrendt L, Czerner C, Gutberlet M, et al. Chronic thromboembolic pulmonary hypertension perioperative monitoring using phase-resolved functional lung (PREFUL)-MRI. *J Magn Reson Imaging*. (2020) 52:610–9. doi: 10.1002/jmri.27097

266. Behrendt L, Voskrebenzev A, Klimes F, Gutberlet M, Winther HB, Kaireit TF, et al. Validation of automated perfusion-weighted phase-resolved functional lung (PREFUL)-MRI in patients with pulmonary diseases. *J Magn Reson Imaging*. (2020) 52:103–14. doi: 10.1002/jmri.27027

267. Kaireit TF, Kern A, Voskrebenzev A, Pohler GH, Klimes F, Behrendt L, et al. Flow volume loop and regional ventilation assessment using phase-resolved functional lung (PREFUL) MRI: comparison with (129)xenon ventilation MRI and lung function testing. *J Magn Reson Imaging*. (2021) 53:1092–105. doi: 10.1002/jmri.27452

268. Marshall H, Voskrebenzev A, Smith LJ, Biancardi AM, Kern AL, Collier GJ, et al. (129) Xe and free-breathing (1) H ventilation MRI in patients with cystic fibrosis: a dual-center study. *J Magn Reson Imaging*. (2022). doi: 10.1002/jmri.28470

269. Klimes F, Voskrebenzev A, Gutberlet M, Kern AL, Behrendt L, Grimm R, et al. 3D phase-resolved functional lung ventilation MR imaging in healthy volunteers and patients with chronic pulmonary disease. *Magn Reson Med*. (2021) 85:912–25. doi: 10.1002/mrm.28482

270. Mendes Pereira L, Wech T, Weng AM, Kestler C, Veldhoen S, Bley TA, et al. UTE-SENCEFUL: first results for 3D high-resolution lung ventilation imaging. *Magn Reson Med*. (2019) 81:2464–73. doi: 10.1002/mrm.27576

271. Klimes F, Voskrebenzev A, Gutberlet M, Obert AJ, Pohler GH, Grimm R, et al. Repeatability of dynamic 3D phase-resolved functional lung (PREFUL) ventilation MR imaging in patients with chronic obstructive pulmonary disease and healthy volunteers. *J Magn Reson Imaging*. (2021) 54:618–29. doi: 10.1002/jmri.27543

272. Glandorf J, Klimes F, Voskrebenzev A, Gutberlet M, Behrendt L, Crisosto C, et al. Comparison of phase-resolved functional lung (PREFUL) MRI derived perfusion and ventilation parameters at 1.5T and 3T in healthy volunteers. *PLoS One*. (2020) 15:e0244638. doi: 10.1371/journal.pone.0244638

273. Kaireit TF, Voskrebenzev A, Gutberlet M, Freise J, Jobst B, Kauczor HU, et al. Comparison of quantitative regional perfusion-weighted phase resolved functional lung (PREFUL) MRI with dynamic gadolinium-enhanced regional pulmonary perfusion MRI in COPD patients. *J Magn Reson Imaging*. (2019) 49:1122–32. doi: 10.1002/jmri.26342

274. Behrendt L, Smith LJ, Voskrebenzev A, Klimes F, Kaireit TF, Pohler GH, et al. A dual center and dual vendor comparison study of automated perfusion-weighted phase-resolved functional lung magnetic resonance imaging with dynamic contrast-enhanced magnetic resonance imaging in patients with cystic fibrosis. *Pulm Circ*. (2022) 12:e12054. doi: 10.1002/pul2.12054

275. Santyr G, Kanhere N, Morgado F, Rayment JH, Ratjen F, Couch MJ. Hyperpolarized gas magnetic resonance imaging of pediatric cystic fibrosis lung disease. *Acad Radiol*. (2019) 26:344–54. doi: 10.1016/j.acra.2018.04.024

276. Mahmood K, Ebner L, He M, Robertson SH, Wang Z, McAdams HP, et al. Novel magnetic resonance imaging for assessment of bronchial stenosis in lung transplant recipients. *Am J Transplant*. (2017) 17:1895–904. doi: 10.1111/ajt.14287

277. Song EJ, Kelsey CR, Driehuys B, Rankine L. Functional airway obstruction observed with hyperpolarized ^{129}xenon-MRI. *J Med Imaging Radiat Oncol*. (2018) 62:91–3. doi: 10.1111/1754-9485.12660

278. Hall CS, Quirk JD, Goss CW, Lew D, Kozlowski J, Thomen RP, et al. Single-session bronchial Thermoplasty guided by (129)Xe magnetic resonance imaging. A pilot randomized controlled clinical trial. *Am J Respir Crit Care Med*. (2020) 202:524–34. doi: 10.1164/rccm.201905-1021OC

279. Svenningsen S, Nair P, Eddy RL, McIntosh MJ, Kjarsgaard M, Lim HF, et al. Bronchial thermoplasty guided by hyperpolarised gas magnetic resonance imaging in adults with severe asthma: a 1-year pilot randomised trial. *ERJ Open Res*. (2021) 7:00268-2021. doi: 10.1183/23120541.00268-2021

280. Adams CJ, DPI C, Di Cesare R, DG MC, Parraga GCanadian Respiratory Research N. On the potential role of MRI biomarkers of COPD to guide Bronchoscopic lung volume reduction. *Acad Radiol*. (2018) 25:159–68. doi: 10.1016/j.acra.2017.08.010

281. Hamedani H, Ma K, DiBardino D, Baron R, Kadlecek S, Amzajerdian F, et al. Simultaneous imaging of ventilation and gas exchange with hyperpolarized (129)Xe MRI for monitoring patients with endobronchial valve interventions. *Am J Respir Crit Care Med*. (2022) 205:e48–50. doi: 10.1164/rccm.202106-1395IM

282. Niedbalski PJ, Hall CS, Castro M, Eddy RL, Rayment JH, Svenningsen S, et al. Protocols for multi-site trials using hyperpolarized (129) Xe MRI for imaging of ventilation, alveolar-airspace size, and gas exchange: a position paper from the (129) Xe MRI clinical trials consortium. *Magn Reson Med*. (2021) 86:2966–86. doi: 10.1002/mrm.28985

283. Wiid J, Smith L, Horn F, Collier G, Swift A, Stewart N, et al. Hyperpolarised gas MR lung imaging. Breaks through to clinical practice. In: *European Respiratory Society International Congress*; Amsterdam. (2015).

284. Norquay G, Collier GJ, Rodgers OI, Gill AB, Screaton NJ, Wild J. Standalone portable xenon-129 hyperpolariser for multicentre clinical magnetic resonance imaging of the lungs. *Br J Radiol*. (2022) 95:20210872. doi: 10.1259/bjr.20210872

285. Grist JT, Collier GJ, Walters H, Kim M, Chen M, Abu Eid G, et al. Lung abnormalities depicted with hyperpolarized xenon MRI in patients with long COVID. *Radiology*. (2022) 305:709–17. doi: 10.1148/radiol.220069

286. Friedman HL. The solubilities of sulfur hexafluoride in water and of the rare gases, sulfur hexafluoride and osmium tetroxide in nitromethane. *J Am Chem Soc*. (1954) 76:3294–7. doi: 10.1021/ja01641a065

287. Wen W-Y, Muccitelli JA. Thermodynamics of some perfluorocarbon gases in water. *J Solut Chem*. (1979) 8:225–46. doi: 10.1007/BF00648882

288. Carrero-Gonzalez L, Kaulisch T, Stiller D. In vivo diffusion-weighted MRI using perfluorinated gases: ADC comparison between healthy and elastase-treated rat lungs. *Magn Reson Med*. (2013) 70:1761–4. doi: 10.1002/mrm.24627

289. Chang YV, Conradi MS. Relaxation and diffusion of perfluorocarbon gas mixtures with oxygen for lung MRI. *J Magn Reson*. (2006) 181:191–8. doi: 10.1016/j.jmr.2006.04.003

290. Ruiz-Cabello J, Perez-Sanchez JM, Perez de Alejo R, Rodriguez I, Gonzalez-Mangado N, Peces-Barba G, et al. Diffusion-weighted 19F-MRI of lung periphery: influence of pressure and air-SF6 composition on apparent diffusion coefficients. *Respir Physiol Neurobiol*. (2005) 148:43–56. doi: 10.1016/j.resp.2005.04.007

291. United states environmental protection agency. Overview of greenhouse gases (2022). updated 16/05/2022. Available at: https://www.epa.gov/ghgemissions/overview-greenhouse-gases

292. Halaweish AF, Charles HC. Physiorack: an integrated MRI safe/conditional, gas delivery, respiratory gating, and subject monitoring solution for structural and functional assessments of pulmonary function. *J Magn Reson Imaging*. (2014) 39:735–41. doi: 10.1002/jmri.24219

293. Jakob PM, Wang T, Schultz G, Hebestreit H, Hebestreit A, Hahn D. Assessment of human pulmonary function using oxygen-enhanced T(1) imaging in patients with cystic fibrosis. *Magn Reson Med*. (2004) 51:1009–16. doi: 10.1002/mrm.20051

294. Hirsch FW, Sorge I, Vogel-Claussen J, Roth C, Grafe D, Pats A, et al. The current status and further prospects for lung magnetic resonance imaging in pediatric radiology. *Pediatr Radiol*. (2020) 50:734–49. doi: 10.1007/s00247-019-04594-z

295. Zanette B, Schrauben EM, Munidasa S, Goolaub DS, Singh A, Coblentz A, et al. Clinical feasibility of structural and functional MRI in free-breathing neonates and infants. *J Magn Reson Imaging*. (2022) 55:1696–707. doi: 10.1002/jmri.28165

296. Dyke JP, Voskrebenzev A, Blatt LK, Vogel-Claussen J, Grimm R, Worgall S, et al. Assessment of lung ventilation of premature infants with bronchopulmonary dysplasia at 1.5 tesla using phase-resolved functional lung magnetic resonance imaging. *Pediatr Radiol*. (2023). doi: 10.1007/s00247-023-05598-6

297. Bauman G, Puderbach M, Heimann T, Kopp-Schneider A, Fritzsching E, Mall MA, et al. Validation of Fourier decomposition MRI with dynamic contrast-enhanced MRI using visual and automated scoring of pulmonary perfusion in young cystic fibrosis patients. *Eur J Radiol*. (2013) 82:2371–7. doi: 10.1016/j.ejrad.2013.08.018

298. Nyilas S, Bauman G, Pusterla O, Ramsey K, Singer F, Stranzinger E, et al. Ventilation and perfusion assessed by functional MRI in children with CF: reproducibility in comparison to lung function. *J Cyst Fibros*. (2019) 18:543–50. doi: 10.1016/j.jcf.2018.10.003